The Cryosphere, 20, 6855–6882, 2026
https://doi.org/10.5194/tc-20-6855-2026
© Author(s) 2026. This work is distributed under
the Creative Commons Attribution 4.0 License.

The Cryosphere Open Access EGU

Estimating the impact of ice-sheet surface height and ice-divide variability on ice-core based climate reconstructions

Christian Wirths[1,2], **Kyung-Sook Yun**[3,4], **Axel Timmermann**[3,4], **Hubertus Fischer**[1,2], **Thomas F. Stocker**[1,2], **and Johannes C. R. Sutter**[1,2]

[1]Climate and Environmental Physics, University of Bern, Bern, Switzerland
[2]Oeschger Centre for Climate Change Research, University of Bern, Bern, Switzerland
[3]Center for Climate Physics, Institute for Basic Science (IBS), Busan, Republic of Korea
[4]Pusan National University, Busan, Republic of Korea

Correspondence: Christian Wirths (christian.wirths@unibe.ch)

Received: 16 July 2026 – Discussion started: 23 July 2026
Revised: 15 October 2026 – Accepted: 12 November 2026 – Published: 23 November 2026

Abstract. Antarctic ice cores are a unique and invaluable archive of past climatic changes over the Antarctic ice sheet. However, as reconstructions are based on the history of surface climate at the ice-core site, variations of the surface geometry and the ice-flow patterns might result in biases within those reconstructions. In this study, we use results from three transient ice-sheet model simulations covering the last two million years to investigate surface-height and ice-divide variability for major Antarctic ice-core sites and for the prospective oldest-ice drilling locations at Little Dome C, Dome Fuji and Dome A. We find that East Antarctic ice-core site elevations varied by up to 240 m over the glacial cycles of the last 800 kyr, whereas glacial–interglacial surface-elevation variability is substantially smaller during earlier periods relevant to prospective oldest-ice sites. Simulations using different ice-sheet models and climate-forcing approaches produce substantially different long-term surface-elevation trends. We further investigate the synchronicity between Antarctic climatic change and simulated surface-height variability and find a substantial shift between the timing of maximum interglacial temperature and ice surface elevation. Furthermore, we quantify the variability of the ice-divide and ice-dome position throughout the time period of the individual ice cores and up to 2 Ma before present for prospective oldest-ice cores, which varies by up to 120 km. Our study suggests that uncertainty in ice surface height has to be taken into account when investigating ice-core based Antarctic temperature reconstructions. Furthermore, the results presented in this study serve as initial constraints for further simplified (e.g. 1D) and higher-resolution regional simulations of Antarctic ice-sheet dynamics at ice-core locations.

1 Introduction

Ice-core based paleo-reconstructions of temperature at ice-core sites serve as an invaluable archive of past climatic changes. In particular, the combination of long continuous records, up to 800 thousand years (EPICA community members, 2004) and now extending to approximately 1.2 million years with the Beyond EPICA Oldest Ice core at Little Dome C (Barbante, 2025), and their high temporal resolution enable studies of climate variability from centennial to orbital time scales, i.e. from centuries to the roughly 20, 41 and 100 kyr periodicities of precession, obliquity and eccentricity (Brook and Buizert, 2018). While past atmospheric composition (e.g. greenhouse gas concentrations) is retrieved from air bubbles within the ice, past temperatures at the ice-core site are derived from one of three approaches: water isotopes within the ice itself (Jouzel et al., 2007), the age difference Δage between the air bubble and the surrounding ice, or measured temperatures within the ice-core borehole (Schwander and Stauffer, 1984; Severinghaus et al., 1998; Kindler et al., 2014; Buizert et al., 2021). However, those reconstructions are subject to various uncertainties. Changing source regions and transport of water vapor (Casado et al., 2018), variations in sea-ice extent (Noone and Simmonds, 2004) or

atmospheric circulation patterns (Kohfeld et al., 2013), together with changing sea surface temperatures (Risi et al., 2010) might have substantial impact on the isotopic composition within the ice core (Buizert et al., 2021). In addition, changes in the ice-sheet topography might influence the Antarctic atmospheric condition and circulation and thus the isotopic precipitation pattern over ice-core locations (Werner et al., 2018; Buizert et al., 2021; Goursaud et al., 2021).

Regardless of the method used to reconstruct past Antarctic surface temperatures, variations in surface elevation, driven by the atmospheric lapse rate, result in differences between the climatic temperature at a constant altitude relative to the present-day geoid (T_{clim}) and the actual surface temperature (T_{S}) as illustrated in Fig. 1. For ice-core locations within the East Antarctic Plateau, low glacial accumulation rates (Parrenin et al., 2016; Bouchet et al., 2023) suggest a reduced surface height during glacials, which would attenuate the observed glacial cooling signal. Conversely, higher-than-present-day accumulation rates during interglacial periods might lead to the opposite effect, where lapse-rate induced cooling at the elevated surface height could diminish the interglacial warming signal. In contrast, at ice-core sites closer to the ice-sheet grounding line, surface-height variations may be primarily influenced by changes in the grounded area driven by ocean dynamics. As a result, the surface could be lower during warm interglacials and higher during cold glacials, thereby amplifying the observed glacial–interglacial temperature variations. The two mechanisms therefore bias the reconstructed glacial–interglacial amplitude with opposite sign, attenuating it on the plateau and amplifying it closer to the grounding line. In addition, an ice sheet does not adjust instantaneously to a change in accumulation or in its boundary conditions, but on its dynamic response time scale, which at interior ice divides scales with the ratio of ice thickness to accumulation rate (Hindmarsh, 1996; Cuffey and Paterson, 2010) and is of the order of up to 10^5 years on the East Antarctic plateau (Cuffey and Paterson, 2010). The surface elevation at an ice-core site is therefore not expected to follow the climatic signal recorded in the ice in phase, and a lag between the two may bias the relative timing of the reconstructed temperature and of other quantities retrieved from the same core. Several studies used ice-sheet model (ISM) simulations to quantify and account for such height changes at different ice-core locations. Early ISM simulations of the Antarctic Ice Sheet (AIS) by Ritz et al. (2001) were utilized to quantify surface-height changes in the Vostok ice-core region. Further regional simulations (Huybrechts et al., 2007) and one-dimensional (1D) ice-sheet models (Parrenin et al., 2007b) were employed to account for potential surface-height variations at the EPICA Dome C (EDC) ice core (Jouzel et al., 2007) and the EPICA Dronning Maud Land (EDML) ice core (Huybrechts et al., 2007; Stenni et al., 2010). Additionally, Cuffey et al. (2016) used surface-height reconstructions and simulations of the West Antarctic Ice Sheet (WAIS) to evaluate their impact on temperature reconstructions from the WAIS Divide ice core (WDC). Ice-sheet model simulations by Sutter et al. (2019) investigated ice-sheet thickness at various Antarctic ice-core sites, supporting the quest for prospective oldest-ice-core sites.

In addition to variations in surface height, the position of the ice divide or ice domes, where ice cores are typically drilled, may have shifted over time. Such shifts could result in ice from different spatial sources being transported to and incorporated into the ice-core column (see Fig. 1). This ice may be influenced by a distinct isotope-temperature relationship, or the paleo-ice divide may have been at a higher elevation, causing a similar type of error as previously described. Notably, this scenario applies to the EPICA Dronning Maud Land (EDML) ice core, a flank site where horizontal advection has transported ice from upstream, higher-elevation deposition sites to the drill location (Huybrechts et al., 2007; Stenni et al., 2010). The position of the ice divide responds to changes in ice-sheet extent and accumulation, among other factors (Weertman, 1973; Anandakrishnan et al., 1994; Hindmarsh, 1996). In these early studies, divide shifts were estimated to range from a few ice thicknesses up to about 50 km. Such migrations leave an imprint on the internal layering (Nereson et al., 1998; Martín et al., 2009).

Nevertheless, earlier ISM simulations and ice-sheet reconstructions are often done on coarse-resolution grids and regional and 1D modeling approaches might not capture the full dynamics of the AIS, in particular the propagated and delayed impact of downstream changes in ice flow. More importantly, no previous study has compared several independent ISMs, driven by different climate-forcing approaches, against each other over the full 2 Myr window at Antarctic ice-core sites. The structural spread of ISM-based surface-height corrections has therefore not been quantified, although such corrections are routinely applied to ice-core temperature reconstructions. In addition, surface-height variations and ice-divide variability have not yet been quantified at all prospective oldest-ice-core drilling sites (Fischer et al., 2013) and for improved bedrock topography maps (Morlighem et al., 2020), but would be important as initial constraints also for 1D-modeling approaches (Parrenin et al., 2007b). In this study, we use three different transient state-of-the-art ISM simulations, covering the last 2 million years of AIS evolution, to quantify ice-sheet surface-height variations and their potential impact on ice-core based temperature reconstructions. As the ice-flow path to the drill site is not explicitly modeled, a shift of the deposition site is assessed only through the variability of the simulated ice-divide and dome position, which indicates at which sites such a shift cannot be excluded. In detail, we aim to answer the following questions: (i) How much do surface-height variations impact ice-core based climate reconstructions across all three ISM simulations? (ii) Is there a de-synchronization between surface-height variations and temperature changes? (iii) How much did the position of the ice divides change at ice-core sites within their covered time span? In the following, we

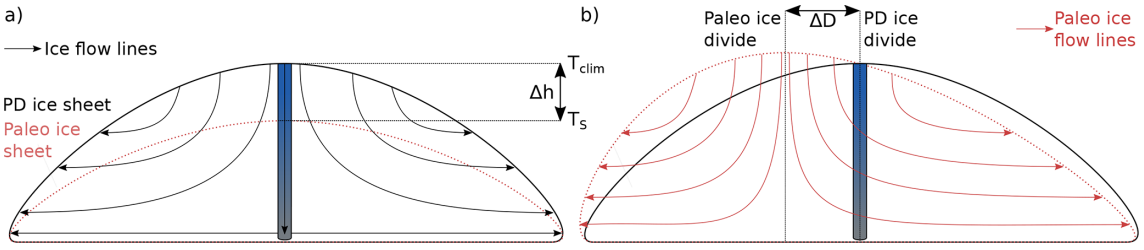


Figure 1. (a) Impact of changing ice-sheet surface height and **(b)** ice-divide location on ice-core based temperature reconstructions. Due to variations in ice-sheet surface height, reconstructed changes in surface temperature at the ice-core site can deviate from the climatic temperature changes (at constant elevation with respect to the present-day geoid). Furthermore, the migration of the ice divide could result in parts of the ice core to originate from a different (higher) location, introducing an additional bias.

will introduce the utilized ISM simulations and how we analyze the ice-sheet–climate synchronization. We then present and discuss the results of our study for various Antarctic ice-core locations with a special emphasis on EPICA Dome C (EDC) and oldest-ice-core locations, especially Little Dome C (LDC).

2 Methods

2.1 Ice-Sheet Modeling

In this study we use ISM simulation results from the two independent ISMs: the Parallel Ice Sheet Model (PISM) (Bueler et al., 2007; Winkelmann et al., 2011) and the Pennsylvania State University Ice Sheet Model (PSUISM) (Pollard and DeConto, 2012a).

2.1.1 PISM-CI

Here, we use PISM simulation results from Wirths et al. (2025) (Config. 1), which uses a climate-index approach, interpolating climate-model snapshots along a paleoclimatic index (Sutter et al., 2019; Wirths et al., 2025), to force the ice-sheet model. Because the fields are linearly interpolated between snapshots, the method captures only a first-order, amplitude-scaled estimate of past temperature and accumulation changes and can only partly reproduce true shifts in the spatial climate patterns. Because the divide position responds to accumulation gradients (Weertman, 1973; Hindmarsh, 1996), which a rescaled fixed pattern can only partly change, the climate-index approach can only reproduce a limited part of the elevation and divide response. To assess the sensitivity to this assumption, an auxiliary PISM simulation was forced with transient simulation data from the Community Earth System Model (CESM) version 1.2 (Yun et al., 2023). In both cases, PISM is run in a hybrid mode using both the shallow ice (SIA) and shallow shelf approximation (SSA) (Winkelmann et al., 2011) on a 16 km horizontal resolution. Basal sliding is described by a pseudo-plastic sliding law (Cuffey and Paterson, 2010), which relates the basal shear stress τ_b to the basal sliding velocity u_b as

$$\tau_b = -\tau_c \frac{u_b}{u_{\text{threshold}}^q |u_b|^{1-q}}, \tag{1}$$

where $u_{\text{threshold}}$ is a threshold velocity and q the pseudo-plastic exponent. The yield stress τ_c is calculated following the Mohr–Coulomb law (Cuffey and Paterson, 2010),

$$\tau_c = c_0 + \tan(\Psi)\ N_{\text{till}} \tag{2}$$

with the till friction angle Ψ, the effective till pressure N_{till} and the "till cohesion" c_0. In both simulations the till friction angle is parametrized as a function of bed elevation below sea level (Winkelmann et al., 2011; Martin et al., 2011; Aschwanden et al., 2013). For a given bed topography $b(x, y)$, Ψ is calculated by

$$\Psi(x,y) = \begin{cases} \Psi_{\min}, & b(x,y) \le b_{\min}, \\ \Psi_{\min} + (b(x,y) - b_{\min})M, & b_{\min} < b(x,y) < b_{\max}, \\ \Psi_{\max}, & b_{\max} \le b(x,y) \end{cases} \tag{3}$$

with minimum and maximum till friction angle ($\Psi_{\min}$, $\Psi_{\max}$), corresponding bed elevations ($b_{\min}$, $b_{\max}$) and gradient $M = (\Psi_{\max} - \Psi_{\min})/(b_{\max} - b_{\min})$. Basal melt in subshelf cavities is calculated through the PICO box model (Reese et al., 2018), which simulates the overturning circulation underneath the ice shelf. Mass loss at the calving front is determined by the physically based 2D-calving parameterization known as Eigen calving (Levermann et al., 2012) in combination with thickness calving removing all ice shelves thinner than $H_{\text{crit}} = 75$ m. The surface mass balance at the ice-atmosphere boundary is calculated using a positive degree day model (Calov and Greve, 2005; Fausto et al., 2009) from precipitation and the surface air temperature forcing. To account for the evolving ice-sheet geometry, the surface air temperature is adjusted with a fixed dry-adiabatic lapse rate (9.8 K km^{-1}) applied to the simulated ice-thickness change, and precipitation is scaled exponentially with this elevation-induced temperature change ($C = 0.07$ K^{-1}; Wirths et al., 2025); an idealized cosine seasonal cycle between annual mean and summer surface air temperature is employed for the degree-day integration. In the simulation from Wirths et al. (2025), hereafter referred to

as PISM-CI, the forcing variables for annual mean surface air temperature, summer surface air temperature, precipitation, ocean temperature and salinity integrated over 300–700 m depth, are derived from snapshots of Community Earth System Models (COSMOS) (Stepanek and Lohmann, 2012) for the Last Glacial Maximum (Zhang et al., 2013), Last Interglacial (Pfeiffer and Lohmann, 2016) and mid-Piacenzian Warm Period (Stepanek et al., 2020) in combination with a climate-index time series representative for the climate evolution of the last 2 million years as described in Wirths et al. (2025) and Sutter et al. (2019). The index is derived from the EDC deuterium record (Jouzel et al., 2007) for the last 800 kyr and the LR04 benthic δ^{18}O stack (Lisiecki and Raymo, 2005) for older periods.

2.1.2 PISM-CESM

As an alternative approach we utilized the identical PISM setup on 16 km resolution but replacing the climate-index based forcing with a recent 3 Ma transient climate simulation results from Yun et al. (2023). In their simulation, Yun et al. (2023) used the CESM version 1.2 on a 3.8° horizontal atmospheric resolution. The model was forced with time-evolving Northern Hemispheric ice-sheet extent retrieved from an intermediate-complexity model (Willeit et al., 2019) and a combination of ice-core based (Lüthi et al., 2008; Bereiter et al., 2015) and simulated (Willeit et al., 2019) atmospheric CO_2 concentrations, in conjunction with orbital forcing from Berger (1978). The Antarctic ice sheet was kept fixed at its present-day configuration throughout the climate simulation. The climate simulation was performed by accelerating the forcings by a factor of 5, and other greenhouse gas forcings beyond the ice-core based coverage were approximated by a regression with the benthic oxygen LR04 stack (Lisiecki and Raymo, 2005; Yun et al., 2023).

To drive the ISM with annual mean and summer surface air temperature as well as the depth-integrated ocean temperature and salinity from the CESM simulation, we correct for potential model biases in CESM. Thus, a forcing variable $T^{i,j}$ at location (i,j) and time t can then be calculated by

$$T^{i,j}(t) = T^{i,j}_{\mathrm{ref}} + \left(T^{i,j}_{\mathrm{CESM}}(t) - T^{i,j}_{\mathrm{CESM,ref}}\right), \tag{4}$$

with reference forcing $T^{i,j}_{\mathrm{ref}}$ and the CESM climate representative for this reference period $T^{i,j}_{\mathrm{CESM,ref}}$. Similarly, we derive the precipitation forcing $P^{i,j}$ by rescaling the reference precipitation pattern as

$$P^{i,j}(t) = P^{i,j}_{\mathrm{ref}} \left(\frac{P^{i,j}_{\mathrm{CESM}}(t)}{P^{i,j}_{\mathrm{CESM,ref}}}\right). \tag{5}$$

For both forcing cases (climate-index approach and transient CESM1.2 forcing) we use the temporal average from 1979–2016 from the Regional Climate Model RACMO2.3p3 (van Dalum et al., 2022) as reference surface air temperature and precipitation as well as the ISMIP6 forcing (Nowicki et al., 2020) as reference forcing for ocean temperature and salinity following Sutter et al. (2019); Wirths et al. (2024, 2025). In both, the PISM-CI and PISM-CESM simulation, geothermal heat flux from Shapiro and Ritzwoller (2004) and sea-level forcing as in Wirths et al. (2024, 2025) were used to drive the model. Bedrock deformation is simulated with the viscoelastic deformable Earth model of Bueler et al. (2007).

2.1.3 PSUISM

In addition to the PISM simulations of the AIS, we use recent simulation data from the PSUISM (Yun and Timmermann, 2026). The model has also been forced with the transient CESM1.2 results (Yun et al., 2023), simulating the AIS on a 20 km resolution using 100 year monthly bias-corrected surface air temperature, precipitation, evaporation, solar radiation and 400 m mean subsurface ocean temperatures. PSUISM applies an analogous bias correction to PISM-CESM, but relative to the 1979–2018 ERA5 climatological mean (Hersbach et al., 2020). Sea level was derived by inter-hemispheric coupling with the additionally simulated northern hemispheric ice sheets as described in Tigchelaar et al. (2018); Yun and Timmermann (2026). PSUISM calculates the surface mass balance from the monthly surface energy balance using the insolation–temperature melt scheme (Robinson et al., 2010). Surface air temperature and precipitation are obtained from the large-scale CESM output and scaled to the evolving PSUISM surface with a fixed lapse-rate correction ($\gamma = 5\,^{\circ}\mathrm{C\,km^{-1}}$) applied to the height difference between the CESM and PSUISM orography. Precipitation is additionally reduced with increasing elevation via a Clausius–Clapeyron factor of $2^{\frac{-\gamma\Delta H}{10\,^{\circ}\mathrm{C}}}$ (Yun and Timmermann, 2026). Bedrock deformation follows an elastic-lithosphere/relaxing-asthenosphere (ELRA) formulation with a single mantle relaxation timescale of 3000 years (Pollard and DeConto, 2012b). In addition, grounding-line ice fluxes and dynamics follow the implementation of Pollard and DeConto (2009, 2012a), based on the theoretical framework of Schoof (2007).

2.1.4 Structural differences between the model setups

Besides the climate forcing, the three simulations differ in several structural choices that directly affect the simulated surface elevation (Table 1). Most importantly, our PISM simulations scale the surface air temperature to the evolving ice-sheet geometry with a dry-adiabatic lapse rate of $9.8\,\mathrm{K\,km^{-1}}$, whereas in PSUISM an empirical lapse rate of $5\,\mathrm{K\,km^{-1}}$ was applied. For a surface-height change of 100 m this amounts to a difference of about 0.5 K in the temperature seen by the surface mass balance scheme, so that the strength of the height–SMB feedback, and with it the amplitude and equilibration

time of the simulated Δh, differ between the models by construction. Bedrock deformation is treated with a viscoelastic Earth model (Bueler et al., 2007) in PISM and with an ELRA formulation with a single relaxation timescale of 3000 years (Pollard and DeConto, 2012b) in PSUISM, which affects the delayed isostatic contribution to Δh.

Each of the three simulations is a single deterministic realization. All values reported in the following are therefore point estimates without formal confidence intervals, and the spread between the three simulations should be read as an indication of structural and forcing-related uncertainty rather than as a statistical uncertainty range.

2.2 Phase analysis

We explore the relationship and synchronicity between surface-elevation anomalies with respect to present-day (Δh) and the climatic signal of the EDC δ^{18}O record (Jouzel et al., 2007) for the last 800 ka and the LR04 benthic δ^{18}O stack (Lisiecki and Raymo, 2005) for time periods older than 800 ka. To do so, we calculate the phase angle $\phi(t)$ of the δ^{18}O time series using the Analytical Signal approach (Gabor, 1946). In general, the analytical signal $x_a(t)$ of a real-valued function $x(t)$ can be expressed by

$$x_a(t) = x(t) + i\mathcal{H}(x(t)) = A(t)e^{i\phi(t)}, \quad (6)$$

with Hilbert transform $\mathcal{H}(x(t))$ of the time series $x(t)$, phase angle $\phi(t)$ and real-valued instantaneous amplitude $A(t)$. For the phase angle to be meaningful, the signal must be sufficiently narrowband to approximately satisfy Bedrosian's product theorem (Honari et al., 2021). We therefore band-pass filter the δ^{18}O record (as well as Δh) to periods of 10–250 kyr using a zero-phase Butterworth filter applied forward and backward, so that the filtering itself introduces no phase shift. The sensitivity of the results to the choice of the filter band is shown in Figs. A1 and A2. Using this decomposition, we then can compare Δh and the climatic signal (δ^{18}O) with respect to the phase angle ϕ as schematically illustrated in Fig. 2 for two ideal cyclical time series. As can be seen, this method allows us to compare the phase synchronization within the signal although the period of the cycles is not constant. This allows us to identify timing of minima and maxima as well as leads and lags of changes between the Antarctic or global climate and Δh.

3 Results

3.1 Surface-elevation variability at ice-core sites

The change of ice surface-elevation anomalies with respect to present-day elevation (Δh) within the three ISM simulations for the last 800 ka at major East Antarctic and the WAIS Divide ice-core sites are illustrated in Fig. 3. At the three continental ice-core sites of EPICA Dome C (EDC), Dome Fuji (DF) and Vostok a similar pattern arises across all three ISM simulations. Warmer interglacial periods are characterized by positive Δh while during glacial periods Δh decreases resulting in the largest negative surface-height anomaly around maximum glacial extent. For the last glacial cycle, changes in Δh (MIS 5–LGM) had an amplitude of 46–138 m for EDC, 21–93 m for DF and 17–104 m for Vostok (see Fig. 4 and Table A1 for additional details). However, changes in Δh lag behind climatic changes, especially in the PSUISM simulation, where we observe ice-sheet growth across the interglacial and far into the glacial periods for EDC, DF and Vostok. Furthermore, we observe that PSUISM generally exhibits higher values of Δh compared to PISM-based simulations. Variability of Δh is dominated by the large-scale 100 kyr glacial–interglacial cycles and modulated by weaker obliquity-paced variability (see Fig. 3b). In contrast, ice-sheet surface-elevation anomalies show substantially higher variability for shorter (precessional) periods at the Talos Dome ice-core site, in particular in simulations forced with the transient CESM climate simulation. For interglacial time periods within the ice-core covered time span all simulations indicate positive Δh at the Talos Dome ice-core site. However, especially during glacials, strong differences in Δh arise across the ISMs. These differences are not even consistent in sign. Overall, Δh at Talos Dome spans from 47–101 (range indicates spread across all simulations) on the upper bound to −50 to −99 on the lower bound. Similar to Talos Dome, Δh variability at the EDML site exhibits more precession-paced variability than the more continental East Antarctic ice cores. However, an overall glacial cycle in Δh arises with slightly positive Δh during interglacials which decrease across glacial periods. At the WDC site, an opposite picture in Δh variability arises. While Δh is increasing during glacial periods, the onset of an interglacial results in a rapid decrease of Δh or a complete collapse of the WAIS, driven by the dynamic response of the ice sheet to enhanced oceanic melt and the crossing of critical stability thresholds within the WAIS basins (Wirths et al., 2025). Importantly, during the last deglaciation we observe a substantial Δh increase between 133–166 m (Holocene–LGM) across all models.

Across all ice-core locations and in between ISM simulations, we observe different timing in local maxima and minima of Δh, as apparent in Fig. 3. To illustrate this further and to relate the timing of Δh peaks and valleys to the phase angle ϕ of the ice-age cycle we use the Analytical Signal approach to illustrate Δh as a function of the phase angle derived from the EDC δ^{18}O record (Jouzel et al., 2007), as shown in Fig. 5. While the EDC δ^{18}O, which serves as proxy for the Antarctic climate (and underlying forcing for the PISM-CI simulation), reaches a minimum for a phase angle between 170–180°, at East Antarctic ice-core sites, simulated Δh reaches its minimum for phase angles larger than 180° especially in the simulations driven by the transient

Table 1. Overview of the model setups of the three ISM simulations. Details and references are given in Sect. 2.1.1 to 2.1.3.

	PISM-CI/PISM-CESM	PSUISM
Horizontal resolution	16 km	20 km
Climate forcing	Climate index (COSMOS snapshots)/transient CESM1.2	Transient CESM1.2
Bias correction reference	RACMO2.3p3 (1979–2016), ISMIP6 ocean	ERA5 (1979–2018)
Ocean forcing	Temperature and salinity, 300–700 m mean	Temperature, 400 m mean
SMB scheme	Positive degree day	Insolation–temperature melt
Lapse rate	9.8 K km^{-1} (dry adiabatic)	5 K km^{-1} (empirical)
Precipitation–height scaling	Exponential, $C = 0.07\,\mathrm{K}^{-1}$	Clausius–Clapeyron factor
Sub-shelf melt	PICO box model	Quadratic parameterization
Ice-cliff failure/hydrofracturing	no	yes
Sea level	Prescribed	Inter-hemispheric ice-sheet coupling
Bedrock deformation	Viscoelastic	ELRA, $\tau = 3000$ years

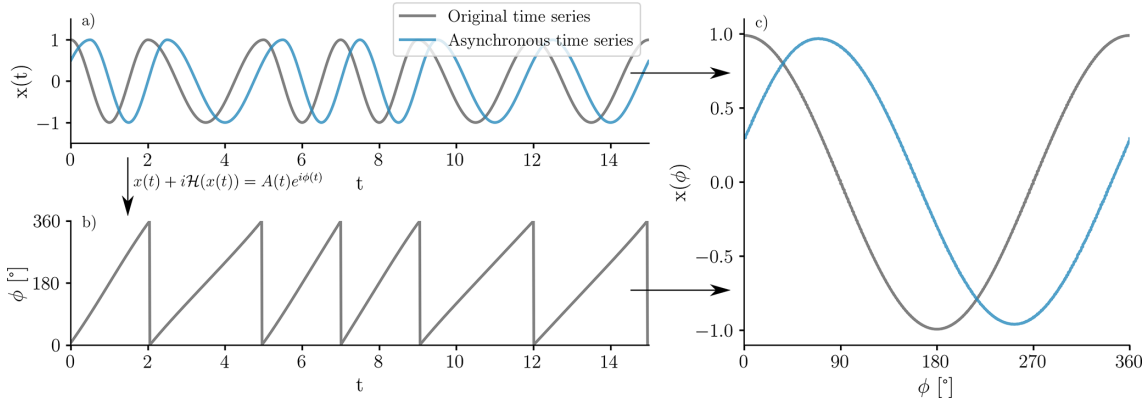


Figure 2. Illustration of the methodology to relate time series to phase dynamics. **(a)** Two example cyclical time series of varying period that are asynchronous with respect to each other; **(b)** phase angle $\phi(t)$ extracted from the original time series via the Hilbert transform-based Analytical Signal approach; **(c)** amplitude-phase relationship for both time series revealed by plotting $x(t)$ against $\phi(t)$.

CESM simulation (PISM-CESM and PSUISM). The timing of Δh maxima shows similar differences between ISM simulations and is delayed with respect to the EDC δ^{18}O signal. This especially becomes apparent for the EDC, DF and Vostok ice-core locations, where the timing of Δh maxima is shifted by several millennia (e.g. up to 48 kyrs for the Last Interglacial peak in PSUISM) between the different ISM simulations and likewise with respect to the δ^{18}O climate record (see Tables A3 and A4 for more details). Across all ice-core sites PISM-CI seems to be most in sync with the δ^{18}O record, while PSUISM exhibits the largest phase shift. Note, however, that the climate index used to force PISM-CI is itself derived from isotope records (Sect. 2.1.1), so that its forcing is in phase with the δ^{18}O record by construction. Any lead or lag simulated by PISM-CI therefore results from the ice-sheet response itself, whereas in PISM-CESM and PSUISM it can additionally reflect the timing of the CESM climate forcing.

3.2 Ice-divide and dome migration

To estimate the variability of the ice-divide position, we track the location of velocity minima near the ice-core site over time. This is achieved by iterating through the depth-integrated velocity field (only in both PISM simulations due to the lack of corresponding velocity data from PSUISM) along the x and y directions independently. For each x-coordinate, we identify the corresponding y-coordinate of the velocity minimum as long as it is lower than a threshold velocity of $\overline{u}_{\mathrm{max}} = 0.5\,\mathrm{m\,yr}^{-1}$, and vice versa. As the divide does not coincide with a grid cell of zero velocity, this threshold is chosen to keep the detected divide as narrow as possible while capturing it almost continuously at all sites. The sensitivity of the ice-divide location to $\overline{u}_{\mathrm{max}}$ is shown in Figs. A3 and A4. This process produces a two-dimensional map that represents our estimate of the ice-divide position. Furthermore, we track the position of the ice dome at or close to the borehole site by finding the location of the local surface-height maxima. Figure 6 illustrates the temporal

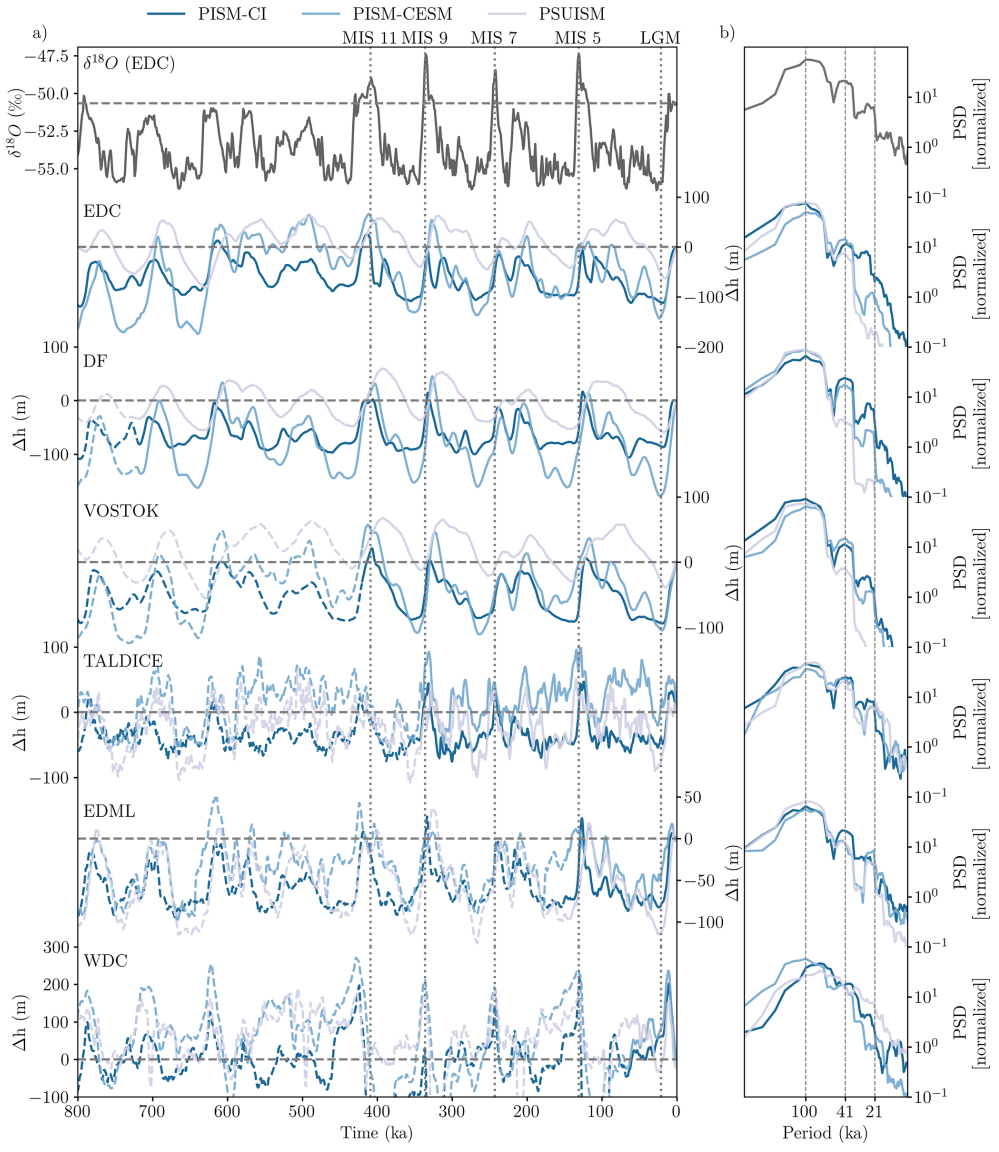


Figure 3. (a) Evolution of the Antarctic climate represented by the EDC δ^{18}O record (Jouzel et al., 2007) and ice-sheet height anomalies over the last 800 ka for the EPICA Dome C (EDC), Dome Fuji (DF), Vostok, Talos Dome (TALDICE), EPICA Dronning Maud Land (EDML) and WAIS Divide (WDC) ice-core location for all three ISM simulations. The colored dashed lines mark time periods which are not covered by the ice-core record. The vertical dotted lines indicate the Last Glacial Maximum (LGM, ∼ 21 ka BP), the beginning of MIS 5 (∼ 130 ka BP), MIS 7 (∼ 243 ka BP), MIS 9 (∼ 336 ka BP) and MIS 11 (∼ 409 ka BP). **(b)** Power Spectral Density (PSD) of the time series shown in **(a)**. The vertical dotted lines indicate a periodicity of 100, 41 and 21 kyrs.

composite of the ice-divide (shading) and ice-dome (marker) position together with the simulated present-day velocity field within the PISM-CI simulation for the six ice-core sites discussed above. While the ice-divide and dome positions do not perfectly align with the real ice-core/dome location for all ISM simulations, there is generally good agreement with differences within a few grid cells. At EDC we observe ice-dome variability of approximately 120 km in PISM-CI and in PISM-CESM, while PISM-CESM is more aligned with the present-day ice-divide position. For Dome Fuji the variability of the ice-dome position narrows down to ∼ 45 km (PISM-CI) and ∼ 70 km (PISM-CESM), respectively. The ice divide at Vostok varies by ∼ 50 km in the PISM-CI and ∼ 65 km in the PISM-CESM simulation. The nearest ice dome varies by ∼ 65 km (PISM-CI) and ∼ 70 km (PISM-CESM). The ice-dome position at Talos Dome disagrees between both PISM simulations. However, throughout the simulation time covered by the Talos Dome ice core, the ice-divide position stays constant (PISM-CESM) or only moves by one grid box (PISM-CI). However, both models fail to simulate the ice-divide position in agreement with the actual ice-core location, due to the generally coarse resolution for the Talos

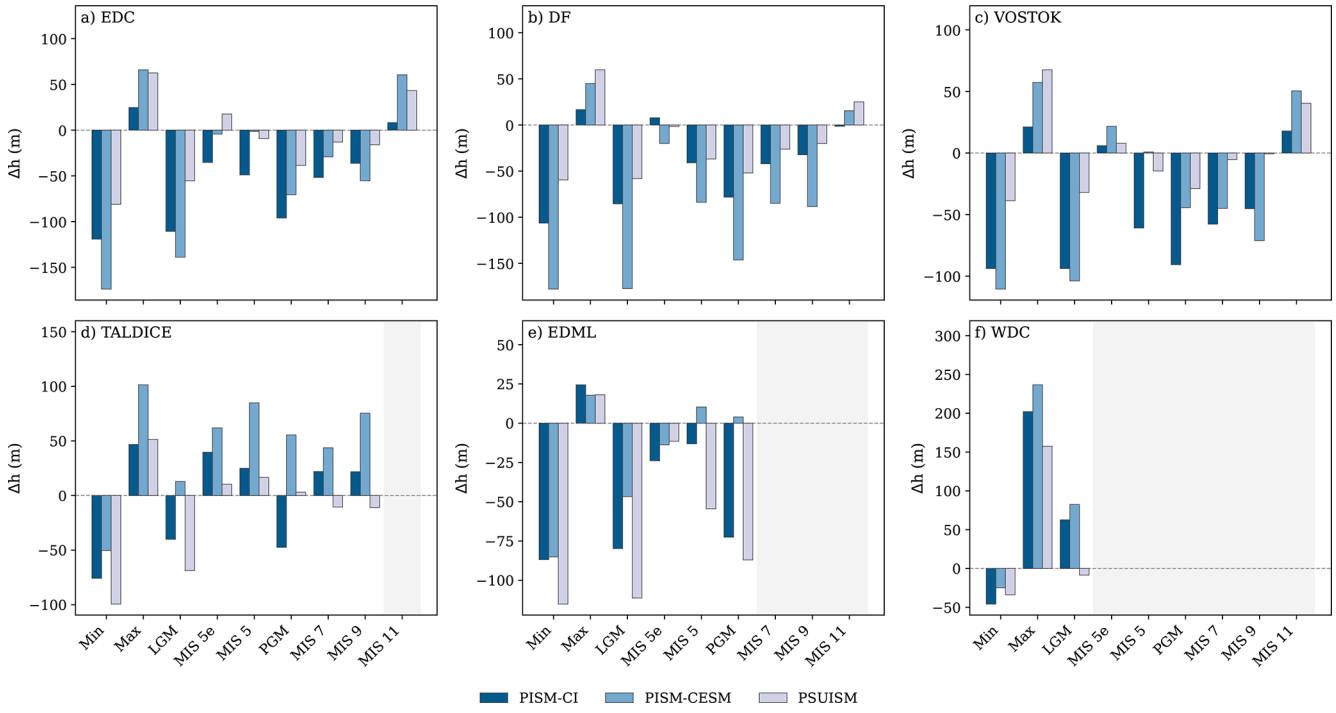


Figure 4. Simulated Δh at the six ice-core sites for PISM-CI, PISM-CESM and PSUISM: minimum and maximum over the period covered by the respective ice-core record, and Δh at the LGM, the end of MIS 5e, MIS 5, the PGM, MIS 7, MIS 9 and MIS 11 (as in Table A1). Grey shading marks time slices older than the respective ice-core record.

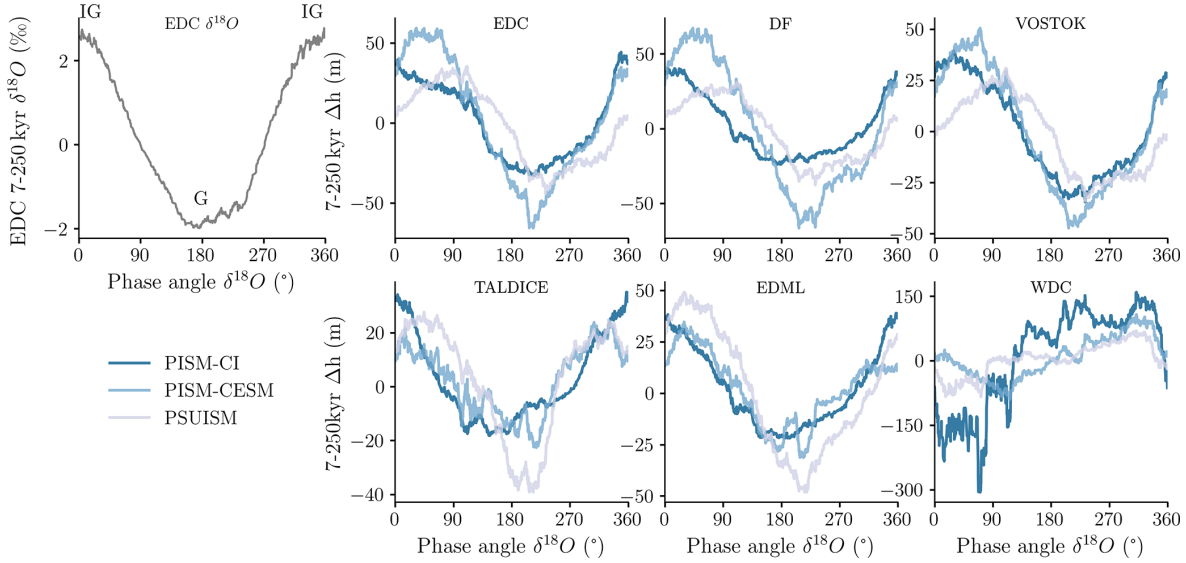


Figure 5. Composite of the bandpass-filtered (periodicity band: 10–250 kyr) EDC δ^{18}O signal (Jouzel et al., 2007) and simulated Δh anomalies as function of phase angle ϕ of the δ^{18}O time series using the Analytical Signal approach. The analysis was performed covering the last 800 kyr regardless of the ice-core covered time period. A phase angle of 0 or 360° here represents interglacial (IG) conditions and around a phase angle of 180° glacial (G) conditions.

Table 2. Simulated variability of the ice-dome position at the ice-core sites over the period covered by the respective ice-core record (upper block) and at the prospective oldest-ice sites between 2.0 and 1.2 Ma BP (lower block). All estimates carry an uncertainty of at least one grid cell (16 km).

Site	Displacement [km]	
	PISM-CI	PISM-CESM
EDC	∼ 120	∼ 120
Dome Fuji	∼ 45	∼ 70
Vostok	∼ 65	∼ 70
Talos Dome	∼ 30	no change
EDML	∼ 120	one grid cell
WDC	∼ 70	∼ 40
LDC	∼ 50	∼ 30
Dome Fuji	∼ 90	∼ 80
Dome A	∼ 50	∼ 50

Dome ice geometry. At the EPICA Dronning Maud Land ice-core site we estimate changes in ice-dome position of up to ∼ 120 km in PISM-CI. However, most of this variability occurs as the ice dome closest to the ice-core drilling site vanishes for several time periods, as the local height maximum flattens into the broader ice-sheet surface. Similarly in the PISM-CESM simulation no local surface-height maximum develops in the vicinity of the ice-core drilling site and the ice-dome position only varies by one grid cell. For WDC we estimated a variability in temporal variability of the ice-dome position of up to ∼ 70 km in PISM-CI and ∼ 40 km in PISM-CESM. Please note that all estimates of ice-divide variations have an uncertainty of at least the grid resolution, which is 16 km. The displacements of all sites are summarized in Table 2. To test whether the dome position depends on the climatic state, we computed the mean dome position separately around the interglacial maxima and the glacial minima of the EDC δ^{18}O record, using its phase angle (Sect. 2.2). The two means differ by less than one grid cell at all sites in both PISM simulations, except for WDC in PISM-CESM (19 km) (Fig. A11). The dome therefore migrates within its envelope throughout the glacial cycle without a systematic glacial or interglacial preference.

In addition, we derived the temperature (see Fig. A7) and surface mass balance (SMB; see Fig. A8) difference between the simulated temporally variable ice-dome position (purple/gray marker in Fig. 6) and the fixed simulated present-day ice-dome position (red marker in Fig. 6) to broadly estimate the order of magnitude of a potential error in ice-core based reconstructions introduced by the variable ice-dome positions. In both cases we used the temperature and SMB forcing fields from each simulation. In particular, the large spatial variability of the ice dome at the EDC site results in temperature fluctuations of up to 1 °C and SMB changes of up to 10 %. For Dome Fuji and Vostok the temperature effect is slightly smaller with ∼ 0.6 and ∼0.4 °C respectively. However, at Vostok the impact of the variable ice-dome location on the SMB is up to 15 %. At Talos Dome, the steep temperature gradient in our forcing data results in a 2 °C temperature change in the PISM-CI simulation, although the ice-dome location varies only by up to ∼ 30 km. At EDML, the large jumps in ice-dome location (see Fig. 6) result in temperature differences of up to 4 °C and SMB changes of over 20 %.

3.3 Implications for Oldest-Ice-Core Sites

We further extend our analysis of ice-core surface-elevation changes towards locations of potential and verified "Oldest Ice" drilling sites that may extend the ice-core records to the last 1.5–2 Myrs. Figure 7 shows the temporal evolution of Δh throughout the last 2 Ma for Little Dome C (LDC), Dome Fuji (DF), and Dome A (DA). Given the small geographic distance between LDC and EDC, we observe the same pattern in Δh variability throughout the last 800 ka at LDC as at EDC. Between 850 to 700 ka BP we observe substantially lower glacial Δh values within the PISM-CESM and PSUISM simulation. In addition we find a lower overall Δh variability before 900 ka in PISM-CESM and PSUISM and before 1.2 Ma in PISM-CI. During the same period the Δh difference between the ISMs increases substantially mostly driven by a long-term trend within the PSUISM simulation. A similar pattern arises for Dome Fuji where PISM-CI indicates a positive long-term surface-height trend in contrast to a negative surface-height trend simulated by PSUISM. For Dome A, we also observe a long-term surface-height growth trend in the PISM-CI simulation. However, PISM-CESM and PSUISM show comparable interglacial Δh values while glacial Δh are substantially lower for the last 800 ka than between 2.0–1.0 Ma BP.

We compare the timing of Δh maxima and minima for the time period between 2.0–1.2 Ma BP for the prospective oldest-ice-core sites using the phase angle retrieved from the LR04 benthic oxygen record (Lisiecki and Raymo, 2005) as shown in Fig. 8. Across all three prospective oldest-ice-core sites, Δh changes of the PISM-CI simulation are synchronous to changes in the benthic oxygen isotopes between 2.0–1.2 Ma BP. Furthermore, the amplitude of glacial–interglacial Δh changes approximately halved when compared with the last 800 kyrs. The PISM-CESM simulation shows a delayed Δh maximum with respect to the benthic oxygen stack but the Δh minimum is reached around a phase angle of 180° for all three oldest-ice-core sites synchronous to the benthic oxygen stack. However, PISM-CESM Δh values remain on a low level beyond a phase angle of 270° and into the glacial termination for DF and DA. The PSUISM simulation shows the smallest Δh variation for all three oldest-ice-core sites. For those sites, maximum Δh values are reached at a phase angle between 70 to 90° (glacial inception) and a minimum arises for phase angles between 180–300° (glacial maximum and glacial termination).

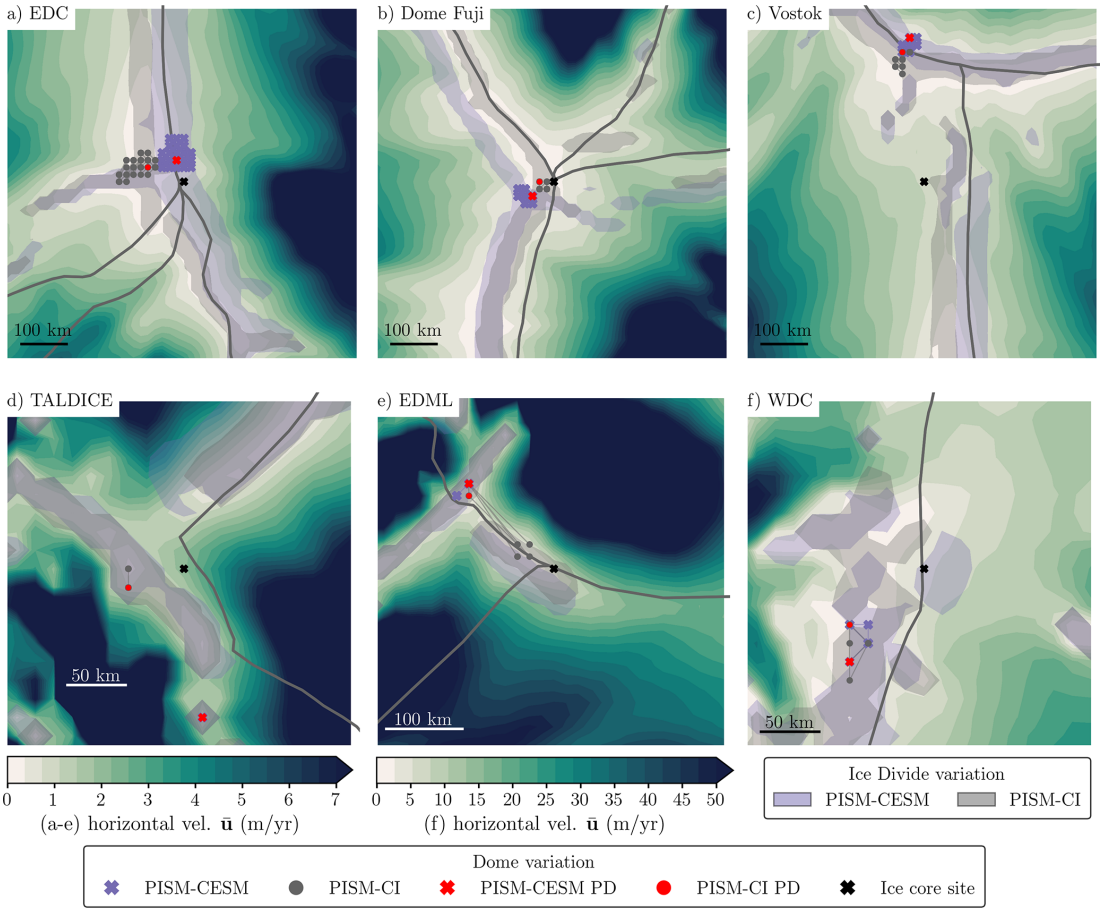


Figure 6. Simulated spatial variation of the ice-divide (shading) and ice-dome (marker) position through the ice-core covered time period (cmp. Fig. 3) for the **(a)** EPICA Dome C (EDC), **(b)** Dome Fuji, **(c)** Vostok, **(d)** Talos Dome, **(e)** EPICA Dronning Maud Land, **(f)** WAIS Divide ice-core domain in the PISM-CI and PISM-CESM simulation. Velocity contours are simulated present-day conditions from the PISM-CI simulation. Thick gray lines indicate the observed present-day ice divide after Rignot et al. (2011). Black cross marks the real drill site location and red markers indicate the simulated present-day ice-dome location.

For all three potential oldest-ice-core sites we probe the variability of the ice-dome and ice-divide position for the time period between 2.0 to 1.2 Ma BP as shown in Fig. 9 (see Fig. A12 for the tracked dome positions). Across that time period, we estimate the spatial variation of the ice dome at LDC to be around ~ 50 km in PISM-CI and ~ 30 km in PISM-CESM. At Dome A, we find similar variability of ~ 50 km in both simulations. At Dome Fuji, we find ice-dome variability of up to ~ 80 km (PISM-CESM) and ~ 90 km (PISM-CI). At all three oldest-ice-core sites, the ice-dome variation leads to a temperature difference of less than 0.5 °C when compared with the fixed simulated present-day ice-dome location (see Fig. A9). While we only observe SMB differences of up to 3 % for LDC, the SMB differs up to 6 % at Dome Fuji and up to 10 % at Dome A between the variable and fixed ice-dome location (see Fig. A10).

4 Discussion

4.1 Impact of surface-height variations on temperature reconstructions

For all East Antarctic ice-core sites investigated in this study, we find glacial–interglacial Δh variations exceeding 100 m for at least one or several ISMs. Depending on the lapse rate, these variations can introduce substantial bias in estimating climatic temperature changes. Increased surface height during interglacial periods causes surface cooling, leading to an underestimation of interglacial warming. Conversely, lower surface height during glacial periods induces a warm bias, thus resulting in underestimation of glacial cooling. In combination, glacial–interglacial climatic temperature changes would be underestimated if Δh variations are not accounted for. In comparison with results from Parrenin et al. (2007b) (see Fig. A6) which were used in the initial temperature reconstruction for EDC (Jouzel et al., 2007), both PISM sim-

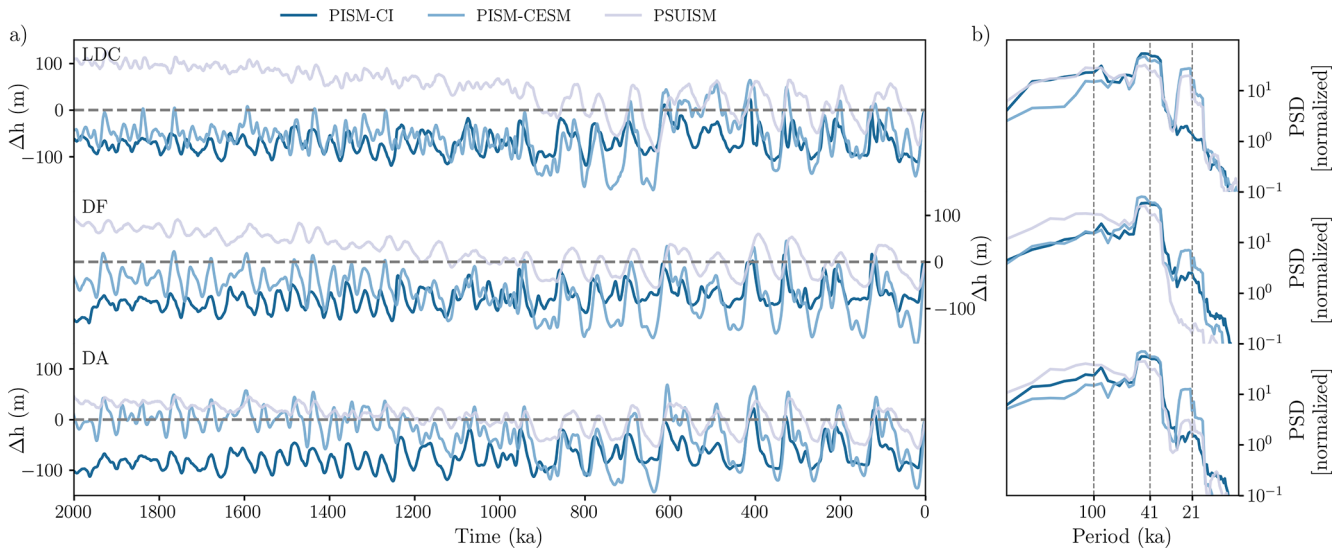


Figure 7. (a) Temporal evolution of the ice-sheet surface-height anomalies over the last 2 Ma for the prospective oldest-ice-core locations at Little Dome C (LDC), Dome Fuji (DF) and Dome A (DA). **(b)** Power Spectral Density (PSD) of the time series in **(a)**. The vertical dotted lines indicate a periodicity of 100, 41 and 21 kyrs.

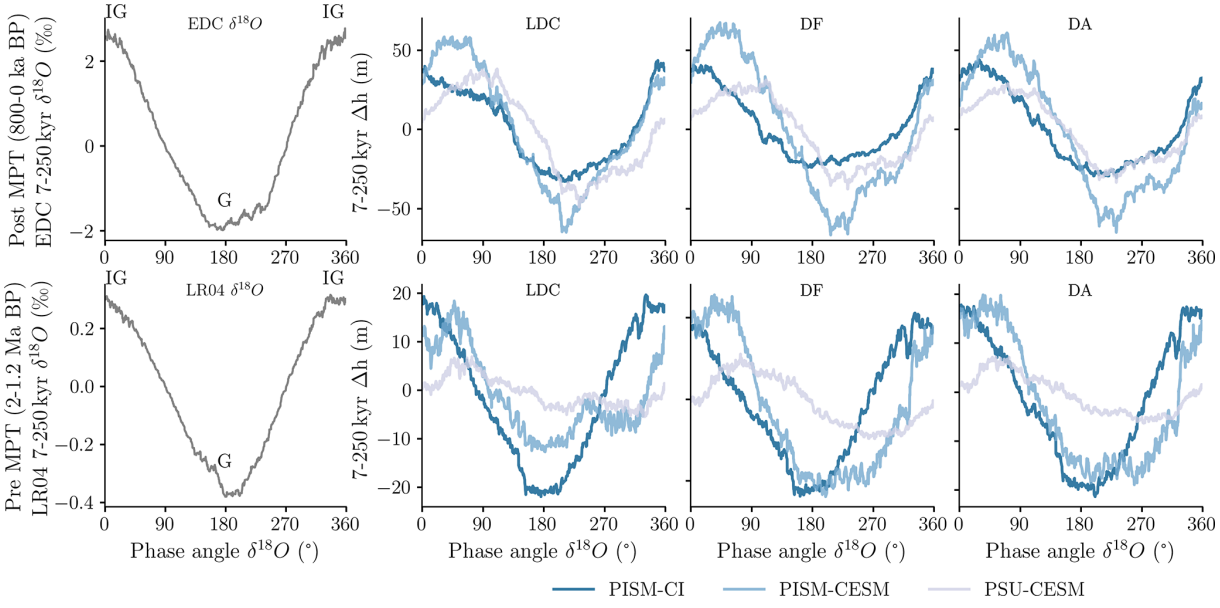


Figure 8. (Top) Composite of the bandpass-filtered (10–250 kyr) EDC δ^{18}O signal (Jouzel et al., 2007) and simulated Δh anomalies at prospective oldest-ice-core sites as function of phase angle ϕ of the δ^{18}O for the last 800 ka. (Bottom) same as above but covering the period from 2.0 Ma to 1.2 Ma BP, using the benthic δ^{18}O LR04 stack (Lisiecki and Raymo, 2005) instead of the EDC δ^{18}O signal.

ulations find similar Δh values for the last four glacial maxima also in agreement with values used in Buizert et al. (2021) and simulated by Sutter et al. (2019). However, substantial differences arise in comparison with PSUISM and for glacial inceptions and early glacials, especially for ice older than 400 ka. This might result in a considerable Δh-induced uncertainty within ice-core based reconstructions. However, at EDC the Δh values of the three simulations have not differed by more than 152 m at any time during the last 800 kyr, where the difference is taken between the largest and the smallest simulated Δh at the same time step. Assuming a dry-adiabatic lapse rate of 9.8 K km^{-1}, this uncertainty ($\sim$ 1.5 K) is around 10 % of the reconstructed maximum glacial–interglacial temperature change at the EDC site of $\sim$ 15 K (Jouzel et al., 2007).

At the WDC site, our simulations support the hypothesis of a WAIS high stand during the early Holocene as also suggested by independent modeling studies (Steig et al., 2001)

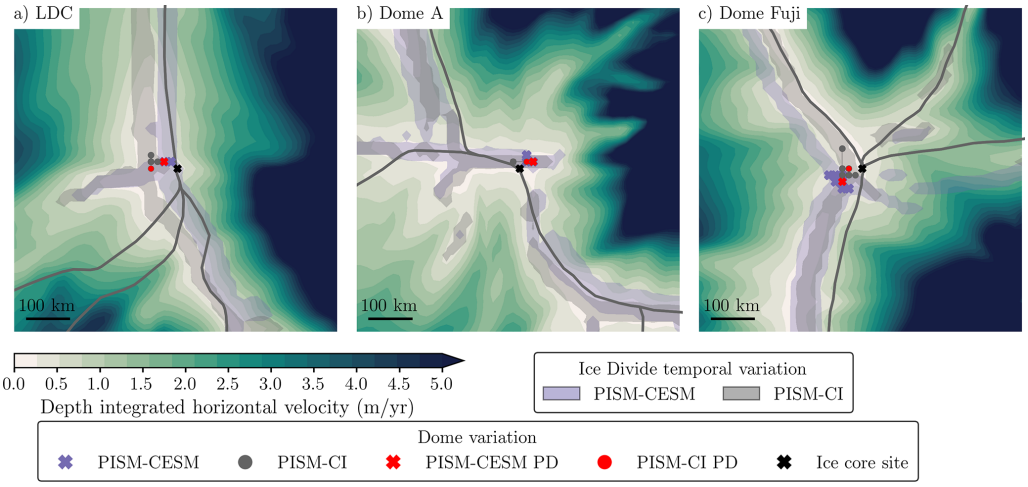


Figure 9. Simulated spatial variation of the ice-divide (shading) and ice-dome (marker) position between 2–1.2 Ma BP for the prospective **(a)** Little Dome C (LDC), **(b)** Dome Fuji, **(c)** Dome A oldest-ice-core domain in the PISM-CI and PISM-CESM simulation. Velocity shading and contours are simulated present-day conditions from the PISM-CI simulation. Thick gray lines indicate the observed present-day ice divide after Rignot et al. (2011). Black cross marks the real drill site location.

and cosmogenic exposure records at nunataks (Ackert et al., 1999). Other modeling studies find higher (Golledge et al., 2014, 2012) and lower (Pollard and DeConto, 2009) WAIS surface during the LGM, emphasizing the substantial spread in simulated surface elevations across ISMs. Nevertheless, increased surface accumulation at WDC during the deglaciation (Fudge et al., 2016), combined with a delayed response to deep ocean warming that triggered increased ice discharge into the ocean, supports our modeled early Holocene surface highstand at the WDC site. From the LGM to the early Holocene, we observe an increase in Δh from 133–166 m within our simulations. Depending on the lapse rate ($\sim$ 7–9.8 K km^{-1}) this would result in cooling bias of 0.9 to 1.6 K. Yet this bias is lower than the uncertainty for the reconstructed LGM to Holocene warming from 9.1–12.4 K (Cuffey et al., 2016). Nevertheless, the consecutive Holocene surface-height decrease might substantially affect reconstructed Holocene temperature changes which range from 0.4–0.8 K (Cuffey et al., 2016).

For all prospective oldest-ice-core sites, we find a diverging long-term trend between the ISMs, resulting in a Δh spread of 150–200 m at LDC for time periods before 1.5 Ma BP. Thus, surface-height changes might be important to correctly quantify Antarctica's long-term temperature trends beyond the Mid-Pleistocene Transition (MPT). However, the glacial–interglacial amplitude at all three prospective oldest-ice-core sites is substantially lowered before 1.2 Ma BP (see Fig. 8), indicating that analysis of glacial–interglacial temperature variations during this time period would be substantially less affected by surface-height variations than during the last 800 kyrs. In addition, our work provides a model reference, which can be used to infer the accumulation rate at the ice-core site (Parrenin et al., 2007b) and to establish an ice-core chronology (Parrenin et al., 2007a; Bouchet et al., 2023).

4.2 Effect of asynchronous ice-core surface elevation and Antarctic temperature

For many East Antarctic ice-core sites we observe a shift in timing of minimum and maximum Δh with respect to the evolution of the Antarctic climate retrieved from the EDC δ^{18}O record, especially in the PSUISM simulation. While parts of this de-synchronization of Antarctic climate and surface-height variation can be attributed to a de-synchronization of the precipitation forcing (see Fig. A5), the de-synchronization is enhanced by the dynamic response of the AIS to climatic changes, chiefly in PSUISM. Such de-synchronization could in theory yield misleading results when the reconstructed Antarctic temperature is compared with other climate variables retrieved from ice cores, like greenhouse gases. For example, the continuous surface-height increase during and beyond the interglacial might result in decreasing reconstructed surface temperature while the climatic temperature stayed constant. If the biased reconstructed surface temperature is then compared for example with the CO_2 record, this initial cooling could be misinterpreted as Antarctic temperature changes leading the CO_2 record. However, for the last 3 interglacials (MIS 5, 7 and 9) at EDC we find that the ice-sheet growth rate was smaller than 13.1 m per millennium (see Table A5 for other ice-core sites) indicating that a cooling trend larger than 0.13 K per millennium (assuming a lapse rate of 9.8 K km^{-1} as an upper bound) could not solely be created by a surface-height change itself. Similarly, for the Last and Penultimate Glacial Maximum, we find a maximum surface-height decrease rate

of 2.5 m per millennium indicating that a warming larger than 0.02 K per millennium could not be solely explained by changes of the ice-sheet surface height. Those numbers are considerably smaller than observed temperature trends at the onset of glacial inceptions and terminations within Antarctic ice cores (Jouzel et al., 2007; Landais et al., 2021; Markle and Steig, 2022) such that we conclude that the effect of surface-height–climate de-synchronization on reconstructed temperature trends is of secondary importance.

For prospective oldest-ice-core sites, de-synchronization appears slightly weaker. In addition, from 2.0 to 1.2 Ma BP, the surface-height change rate varied between −9.0 to 15.7 m per millennium (see Table A2), which suggests that surface-height–climate de-synchronization has only a minor effect on the analysis of prospective oldest-ice cores. In general, a more precise understanding of the surface-height–climate synchronization is hard to retrieve since Δh depends on local/regional surface accumulation as well as non-local ice dynamics (e.g. grounding-line dynamics). The latter varies between ISM parameterizations, but is also affected by uncertainties in other forcing variables like oceanic warming. Reconstructing accumulation at ice-core sites is equally challenging as initial information on surface-height changes is often required (Parrenin et al., 2007b), which would result in a chicken-and-egg problem.

The diverging long-term trends in Δh most likely result from structural differences between the ISMs rather than from the climate forcing itself, as PISM-CESM and PSUISM are driven by the same transient CESM simulation (Yun et al., 2023) but show different long-term behavior. While both ISMs include an interactive height–SMB feedback (see Sect. 2.1), they differ in the SMB scheme and applied lapse rate (Sect. 2.1.4), the initialization, the treatment of bedrock deformation (viscoelastic Lingle–Clark model vs. ELRA with a single 3000-year relaxation timescale) and the marine ice-sheet dynamics, where PSUISM includes hydrofracturing, ice-cliff failure and a quadratic ocean melt parameterization (Pollard et al., 2015), while PISM uses the PICO box model (Reese et al., 2018). The latter also affects interior sites, as grounding-line changes within the marine Aurora and Wilkes basins can propagate upstream towards the Dome C region (Mengel and Levermann, 2014; Reese et al., 2018; Wirths et al., 2025). However, as no proxy record of absolute surface elevation exists for the East Antarctic ice sheet interior for time periods before the MPT, the diverging trends cannot be validated against observations and the resulting Δh spread of 150–200 m at LDC and the opposite long-term trends at Dome Fuji should be interpreted as structural uncertainty of the simulated Δh. The same structural differences most likely also cause the different response times of the ISMs, as neither the ice rheology (all simulations use a Glen-type flow law) nor a missing height–SMB feedback can explain the long equilibration time of PSUISM (up to 48 kyr for the Last Interglacial Δh maximum at EDC, Table A3).

4.3 Ice-Divide evolution

For all Antarctic ice-core sites, we find considerable variability within the ice-divide and dome positions across both PISM simulations. As these estimates rest on the two PISM simulations only, and PSUISM deviates most strongly from them in the simulated surface-height evolution (Sect. 3.1 and 3.3), the reported displacement of up to about 120 km is likely a lower bound on the spread that a PSUISM-inclusive analysis would show. This implies that the climatic information encapsulated within the ice core can originate from different (but still relatively close) locations within the Antarctic ice sheet. This is of particular importance for spatially variable climate variables such as accumulation and temperature. Our broad estimates of this bias, obtained by comparing temperature and SMB at the variable and fixed present-day ice-dome positions, indicate that the potential bias in reconstructed temperature resulting from ice-dome variability is of the same order of magnitude as biases introduced by surface-height variations. However, these numbers should be considered only as first-order estimates, since the origin of ice segments within an ice core depends on the evolution of the velocity field rather than directly on the ice-dome position. Regional three-dimensional ice-sheet simulations would permit tracing every ice-core segment back to its surface origin as was done for EDML by Huybrechts et al. (2007). However, as the full velocity fields of the three simulations have not been saved on the necessary temporal resolution, we postpone this analysis to future studies with high-resolution regional simulations nested into continental-scale simulations such as those used here. For oldest-ice-core locations, we find a substantially reduced ice-dome variability at LDC, which might be due to the dominance of the 41 kyr glacial–interglacial cycles previous to the MPT. Similarly, we find that a potential bias due to ice-dome variability seems to be substantially lower at LDC previous to the MPT.

4.4 Model limitations

ISM simulations and therefore the results presented in this study are heavily affected by the resolution of the ISMs (Wang et al., 2024), as especially the heterogeneous bedrock topography has an important influence on the ice flow and thus in particular the ice-divide position. Therefore, high-resolution simulations would be more favorable. Nevertheless, those high-resolution simulations are computationally not feasible on a longer time and continental scale. In contrast, purely regional simulations might not capture the full dynamics of the ice sheet as far-field effects (e.g. changing grounding-line position of flux) are not accounted for. Simulations of highly resolved ice-core locations nested within coarser-resolution continental-scale ice-sheet simulation would be desirable, and simulation results from this study could be used as initial constraint of continental-scale ice-sheet dynamics. In addition to the coarse grid resolution,

uncertain knowledge of the climatic boundary conditions at the ice-core site and on continental scale heavily affect the outcome of this study. As uncertainties in climate forcings are known to have a large impact on past, present and future continental-scale ice-sheet simulations (Li et al., 2023; Wirths et al., 2024), climate reconstructions at ice-sheet sites might help as important constraints to improve ice-sheet simulations as a whole. However, as seen in this study those reconstructions are not necessarily independent of the evolution of the ice sheet itself. Ideally, one would therefore retrieve climate and ice-sheet information simultaneously. Using isochrones (layers of same age) within the ice sheet as additional constraint for the ice sheet might permit inverting for both climatic and ice-sheet conditions at the same time (Rieckh et al., 2024).

5 Conclusion

Here, we used results from three different continental ISM simulations of the AIS to investigate the temporal evolution of the ice-sheet surface height and the ice-dome position at key Antarctic ice-core locations up to two million years into the past. Our results showed that surface-height changes could have led to an underestimation of amplitude of glacial–interglacial temperature change, if those changes are not accounted for. Comparison with the commonly used 1D modeling results for the EDC site showed only limited differences with our simulations for maximum glacial extent and interglacial, but substantial differences arose for glacial inceptions and early glacials. Furthermore, we compared the timing of maximum and minimum surface-height anomalies with the evolution of the Antarctic climate and found that ice-sheet height generally lags Antarctic climate during interglacials and glacial inceptions. We further quantified the delayed ice-sheet growth rate during interglacials and glacial inceptions to test if this could affect the timing of the glacial inception recorded within the Antarctic ice cores – which is most likely not the case, given the only small surface-height change rates in our simulations. Finally, we investigated the variability of the ice-divide and ice-dome position across the past, which showed variability of up to 120 km, indicating a potential bias within the ice-core record due to spatially heterogeneous sourced ice segments. The potential bias is largest at EDML, where dome migration changes temperature and SMB by up to 4 °C and 20 %, and least constrained at Talos Dome, where the Δh differences between the ISMs are not consistent in sign. At the East Antarctic plateau sites, Δh variations of the order of 100 m affect the glacial–interglacial amplitude while the dome position is comparatively stable. The prospective oldest-ice sites, in particular LDC before the MPT, are least affected. The results presented in this study will assist ice-core scientists in the interpretation of their results and serve as initial constraints of AIS dynamics for time periods beyond 800 ka BP, supporting the interpretation of further prospective oldest-ice-core records.

Appendix A: Supplementary information

Table A1. Minimum and Maximum Δh anomalies through the ice-core covered time period and Δh for the Last Glacial Maximum (LGM, $\sim$ 21 ka BP), the Penultimate Glacial Maximum ($\sim$ 140 ka BP), the end of MIS 5e ($\sim$ 123 ka BP), MIS 5 ($\sim$ 130 ka BP), MIS 7 ($\sim$ 243 ka BP), MIS 9 ($\sim$ 336 ka BP) and MIS 11 ($\sim$ 409 ka BP).

Ice-core site	ISM	Min Δh [m]	Max Δh [m]	LGM Δh [m]	MIS 5e Δh [m]	MIS 5 Δh [m]	PGM Δh [m]	MIS 7 Δh [m]	MIS 9 Δh [m]	MIS 11 Δh [m]
EDC	PISM-CI	−119	25	−110	−35	−49	−96	−51	−36	8
	PISM-CESM	−173	66	−139	−4	−1	−71	−29	−55	60
	PSUISM	−81	63	−55	18	−9	−39	−13	−16	43
DF	PISM-CI	−106	17	−85	8	−40	−78	−42	−32	−1
	PISM-CESM	−178	45	−177	−20	−84	−146	−85	−88	15
	PSUISM	−60	60	−58	−2	−37	−52	−26	−20	25
Vostok	PISM-CI	−94	21	−93	6	−61	−91	−58	−45	18
	PISM-CESM	−110	57	−103	22	1	−44	−45	−71	50
	PSUISM	−39	68	−32	8	−15	−29	−5	−1	40
TALDICE	PISM-CI	−76	47	−40	40	25	−47	22	22	
	PISM-CESM	−50	101	13	62	85	55	44	75	
	PSUISM	−99	51	−69	10	17	3	−11	−11	
EDML	PISM-CI	−86	24	−80	−24	−13	−73			
	PISM-CESM	−85	18	−47	−14	10	4			
	PSUISM	−115	18	−111	−11	−54	−87			
WDC	PISM-CI	−46	202	63						
	PISM-CESM	−24	237	82						
	PSUISM	−34	158	−8						

Table A2. Minimum and maximum Δh anomalies [m] and minimum and maximum surface-height change rate [m kyr^{-1}] between 2.0 and 1.2 Ma BP at the LDC, DF and Dome A ice-core locations.

Ice-core site	ISM	Min Δh [m]	Max Δh [m]	Min $\frac{dh}{dt}$ [m kyr^{-1}]	Max $\frac{dh}{dt}$ [m kyr^{-1}]
LDC	PISM-CI	−119	−32	−7.1	13.4
	PISM-CESM	−97	8	−9.0	12.5
	PSUISM	47	126	−3.9	6.9
DF	PISM-CI	−131	−29	−5.7	15.7
	PISM-CESM	−104	22	−8.3	13.7
	PSUISM	18	95	−3.7	4.3
Dome A	PISM-CI	−122	−35	−4.6	12.1
	PISM-CESM	−58	57	−7.5	12.9
	PSUISM	0	46	−2.8	3.5

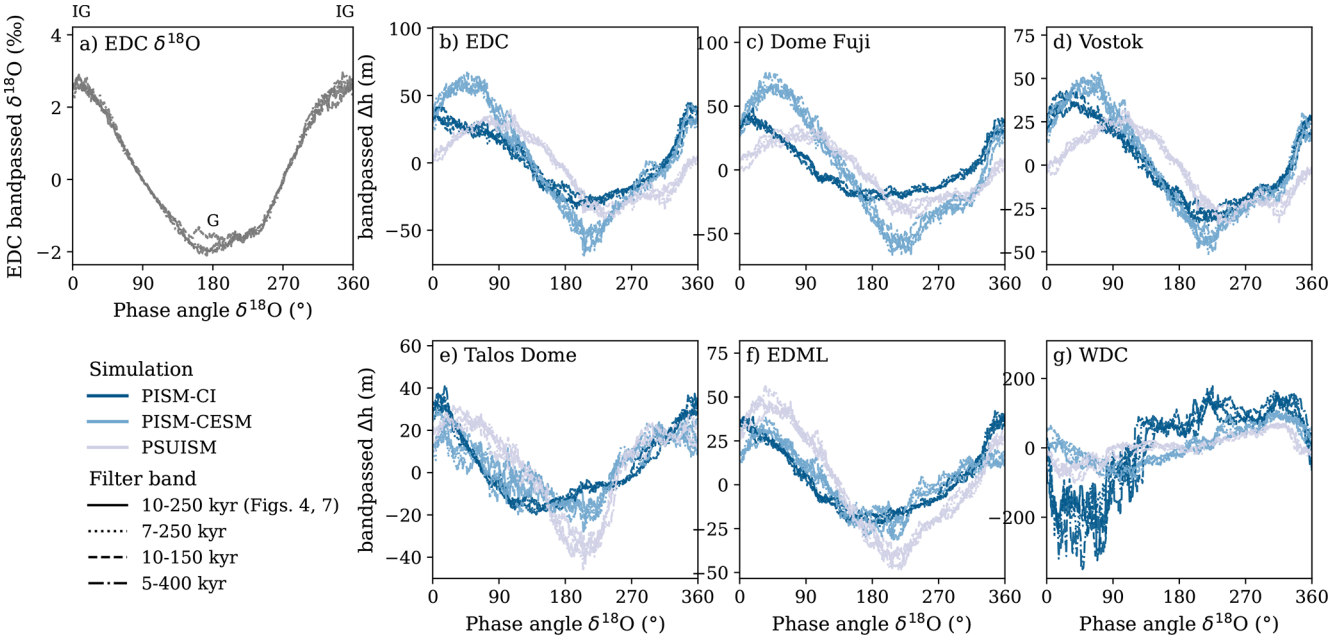


Figure A1. Composite of the bandpass-filtered δ^{18}O record and simulated Δh anomalies as function of the δ^{18}O phase angle, as in Fig. 5 for four filter bands: 10–250 kyr (solid), 7–250 kyr (dotted), 10–150 kyr (dashed) and 5–400 kyr (dash-dotted).

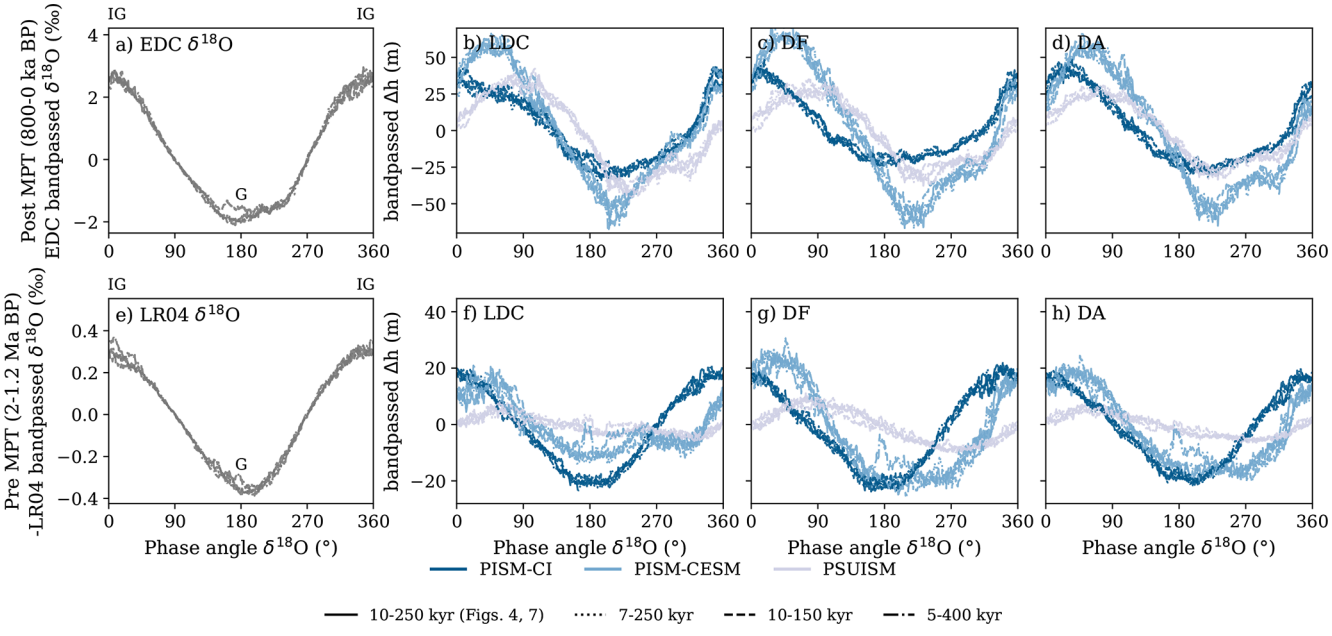


Figure A2. Composite of the bandpass-filtered δ^{18}O record and simulated Δh anomalies as function of the δ^{18}O phase angle, as in Fig. 8 for four filter bands: 10–250 kyr (solid), 7–250 kyr (dotted), 10–150 kyr (dashed) and 5–400 kyr (dash-dotted).

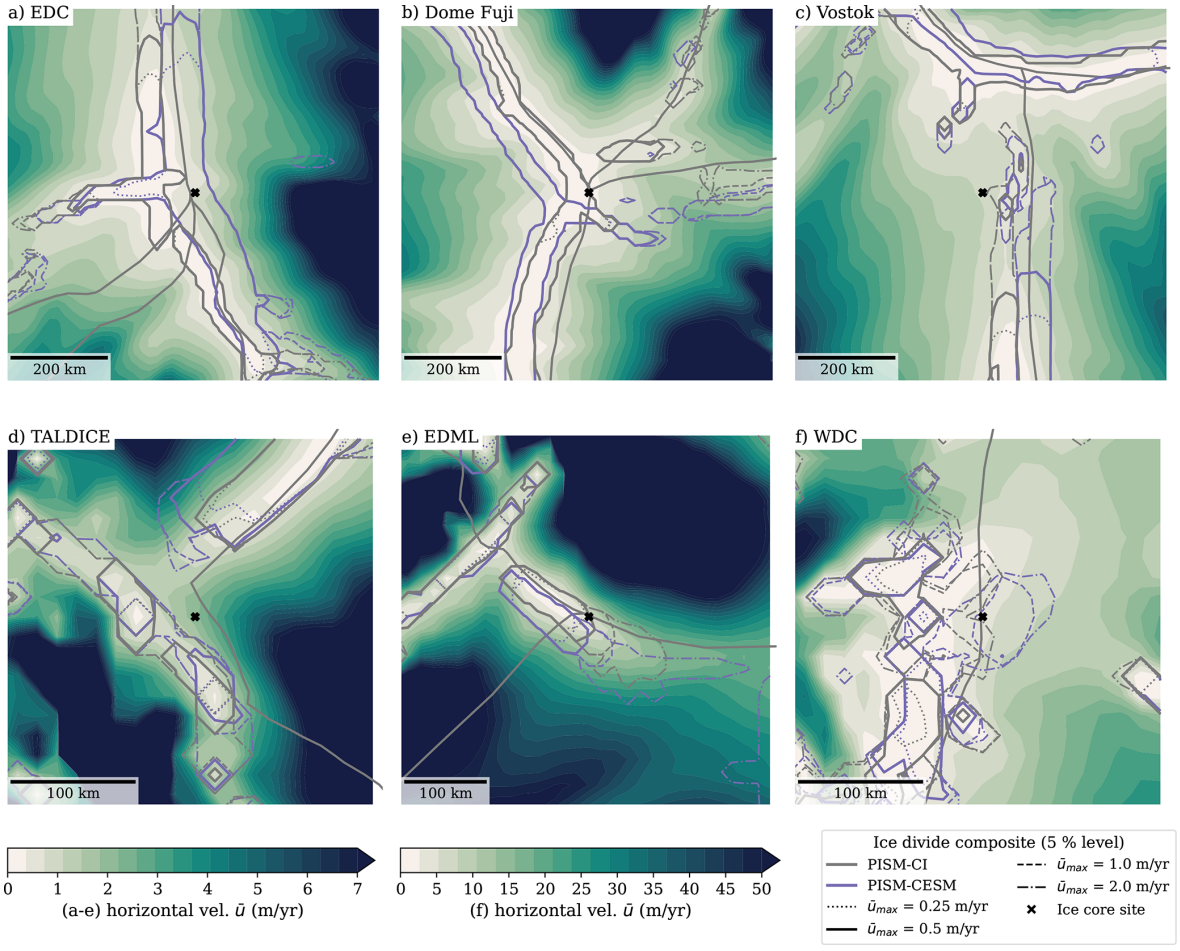


Figure A3. Ice-divide composites as in Fig. 6 for velocity thresholds $\overline{u}_{\max}$ of 0.25, 0.5, 1.0 and 2.0 m yr^{-1} in PISM-CI (grey) and PISM-CESM (purple) over the simulated present-day PISM-CI velocity field. Crosses mark the drill sites.

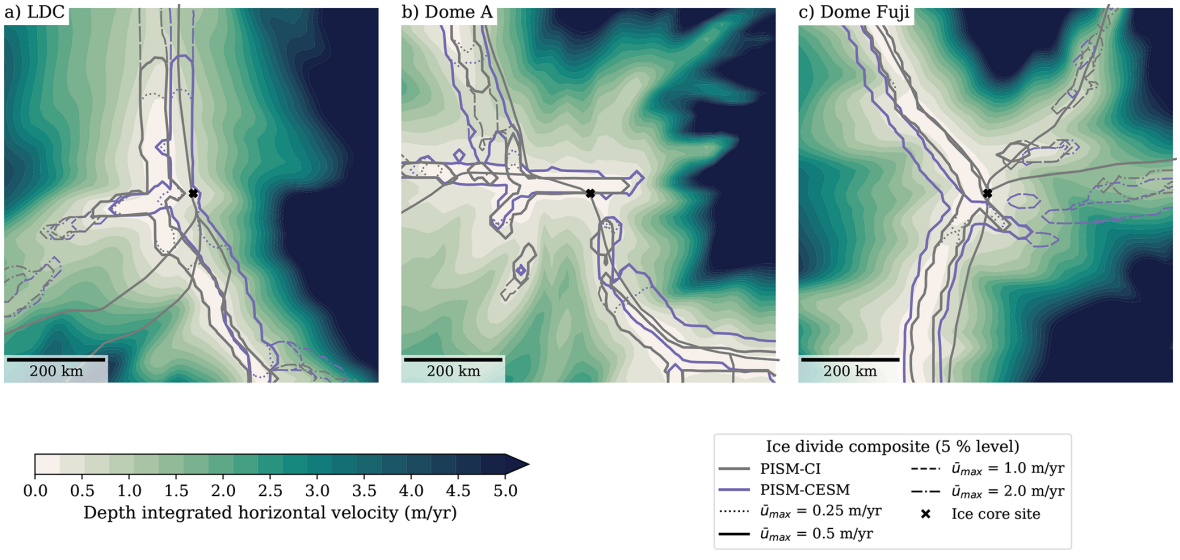


Figure A4. Same as Fig. A3 for the prospective oldest-ice sites between 2.0 and 1.2 Ma BP, as in Fig. 9.

Table A3. Lag of the simulated Δh extrema behind the EDC $\delta^{18}O$ record for individual glacial cycles of the last 800 kyr. Positive values mean that Δh lags the isotope record. Values in parentheses fall outside the period covered by the respective ice-core record; – no Δh minimum within the cycle. All values are point estimates from single deterministic simulations; the range gives the spread between cycles, not an uncertainty.

		Interglacial peaks, lag of Δh maximum [kyr]						Glacial maxima, lag of Δh minimum [kyr]					
Site	ISM	MIS 1	MIS 5e	MIS 7	MIS 9	MIS 11	median (range)	MIS 2	MIS 6	MIS 8	MIS 10	MIS 12	median (range)
EDC	PISM-CI	+6	+4	+6	+2	−5	+4 (−5, +10)	+5	+3	+6	+3	−2	+4 (−2, +10)
	PISM-CESM	+9	+1	+5	+9	−4	+5 (−4, +20)	+1	–	+7	+4	−1	+2 (−1, +11)
	PSUISM	+9	+48	+45	+15	+11	+14 (+1, +48)	+5	−3	+19	+15	+1	+12 (−3, +22)
Dome Fuji	PISM-CI	+5	+6	+5	+3	+1	+4 (−3, +9)	+6	+4	+4	+6	+0	+4 (−2, +6)
	PISM-CESM	+9	+12	+9	+9	+5	+9 (+0, +19)	+4	–	+8	+8	−2	+6 (−2, +17)
	PSUISM	+9	+23	+43	+21	+14	+14 (+3, +43)	+5	−4	+10	+16	+4	+8 (−4, +19)
Vostok	PISM-CI	+9	+9	+8	+5	+0	+7 (−1, +12)	+5	−5	+9	+6	(−2)	+6 (−5, +11)
	PISM-CESM	+9	+13	+8	+12	−5	+9 (−5, +20)	+4	–	+11	+12	(+0)	+11 (+0, +23)
	PSUISM	+9	+23	+47	+22	+14	+22 (+3, +47)	+6	−1	+22	+16	(+3)	+13 (−1, +26)
Talos Dome	PISM-CI	+2	+4	+2	+2	(−15)	+2 (−15, +12)	−4	+1	+3	(−4)	(−2)	−1 (−4, +3)
	PISM-CESM	+2	−4	+0	+3	(+36)	+2 (−4, +36)	−5	+10	+7	(+6)	(−5)	+2 (−5, +10)
	PSUISM	−1	−6	−5	−2	(−7)	−1 (−7, +17)	−5	−5	+4	(+3)	(−4)	−2 (−5, +4)
EDML	PISM-CI	+3	+3	(+4)	(+1)	(−11)	+1 (−11, +8)	+4	−5	(+1)	(−3)	(+5)	−2 (−5, +5)
	PISM-CESM	+2	−3	(+4)	(−1)	(+5)	+2 (−4, +15)	−2	+10	(+6)	(+2)	(+0)	+4 (−3, +43)
	PSUISM	+5	+12	(+7)	(+9)	(+8)	+8 (−2, +17)	+1	−5	(+5)	(+4)	(−2)	+2 (−5, +15)

Table A4. Same as Table A3 for the prospective oldest-ice sites between 2.0 and 1.2 Ma BP, with the LR04 benthic stack as reference.

Site	ISM	Lag of Δh maximum [kyr], median (range)	Lag of Δh minimum [kyr], median (range)
LDC	PISM-CI	+0 (−3, +15)	+0 (−5, +9)
	PISM-CESM	+8 (−5, +19)	+6 (−5, +15)
	PSUISM	+10 (−5, +20)	+8 (−5, +18)
Dome Fuji	PISM-CI	+1 (−5, +15)	+0 (−5, +9)
	PISM-CESM	+8 (−4, +18)	+4 (−2, +9)
	PSUISM	+11 (+0, +19)	+8 (+1, +16)
Dome A	PISM-CI	+2 (−3, +15)	+1 (−3, +9)
	PISM-CESM	+7 (−5, +20)	+5 (−2, +10)
	PSUISM	+10 (−5, +19)	+7 (+0, +15)

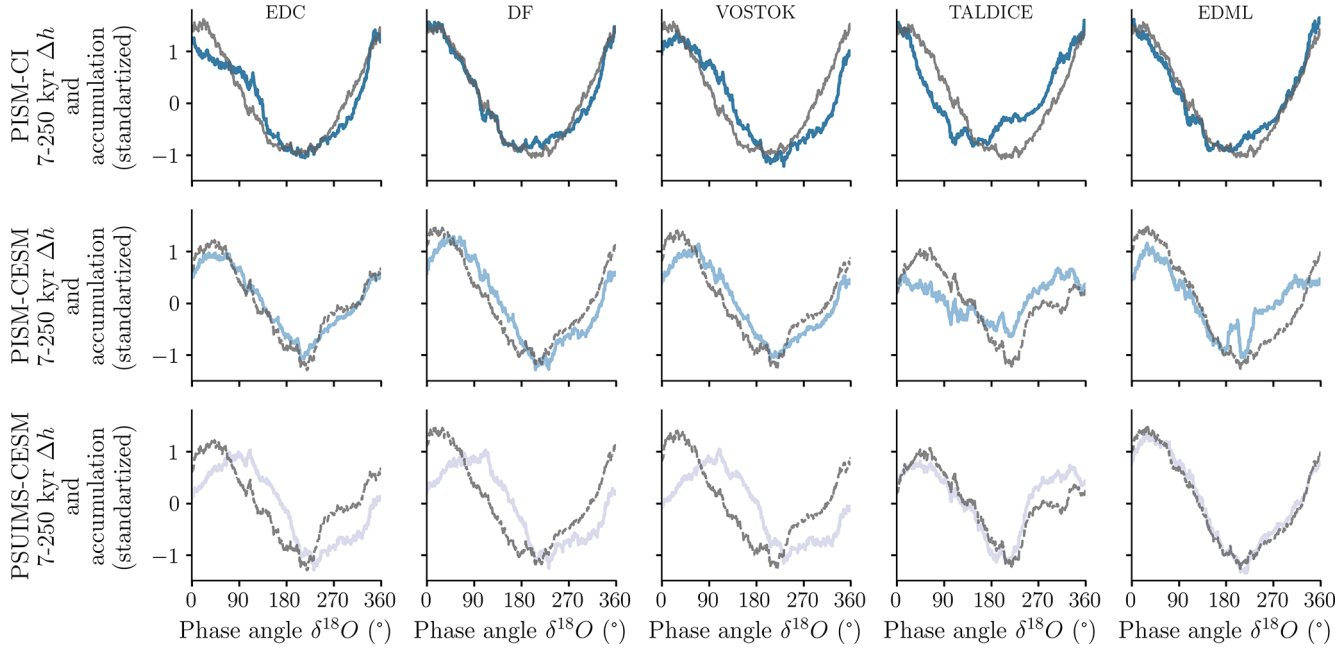


Figure A5. Composite of the bandpass-filtered (10–250 kyr) simulated Δh anomalies (blueish lines) and surface accumulation (dashed gray lines) as function of phase angle ϕ of the EDC δ^{18}O time series using the Analytical Signal approach. The analysis was performed covering the last 800 kyr regardless of the ice-core covered time period. A phase angle of 0 or 360° here represents interglacial conditions and around a phase angle of 180° glacial conditions.

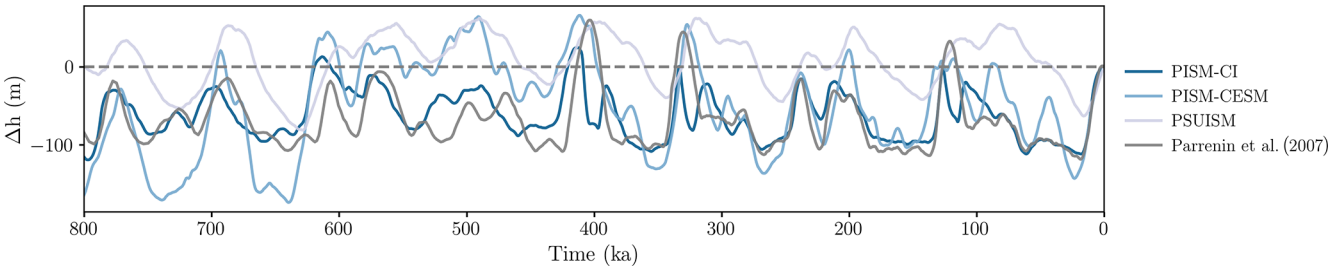


Figure A6. Temporal evolution of the ice-sheet surface-height anomalies over the last 800 ka for the EDC site, simulated in this study (blueish lines) and from a 1D modeling approach (Parrenin et al., 2007b) utilized to correct EDC temperature reconstructions (Jouzel et al., 2007).

Table A5. Minimal and maximal surface-height change rate for the EDC, DF and Vostok ice-core sites for time periods during and after the LGM as well as during time periods around the last three glacial inceptions of MIS 5, 7 and 9.

Ice-core site	ISM	LGM (21–15 ka BP) [m kyr^{-1}]		MIS 5 (125–110 ka BP) [m kyr^{-1}]		MIS 7 (240–228 ka BP) [m kyr^{-1}]		MIS 9 (336–321 ka BP) [m kyr^{-1}]	
		Max	Min	Max	Min	Max	Min	Max	Min
EDC	PISM-CI	4.6	−0.6	13.1	−13.3	5.2	−6.6	−2.5	−16.1
	PISM-CESM	8.6	3.5	4.2	−5.4	3.5	−7.9	17.2	−4.6
	PSUISM	0.6	−2.5	4.1	−0.16	4.5	−1.5	11.1	3.8
DF	PISM-CI	3.1	−0.6	−3.1	−7.2	2.7	−6.4	−3.6	−7.9
	PISM-CESM	6.5	1.2	11.0	−9.3	8.3	−4.9	19.9	−5.4
	PSUISM	1.0	−0.8	4.8	1.22	4.2	0.0	7.4	4.5
Vostok	PISM-CI	3.0	0	7.0	−4.0	5.3	−3.1	3.9	−3.5
	PISM-CESM	4.8	−0.7	3.5	−6.2	3.5	−3.0	14.1	3.3
	PSUISM	−0.1	−2.1	4.1	1.0	3.3	−0.2	6.5	3.3

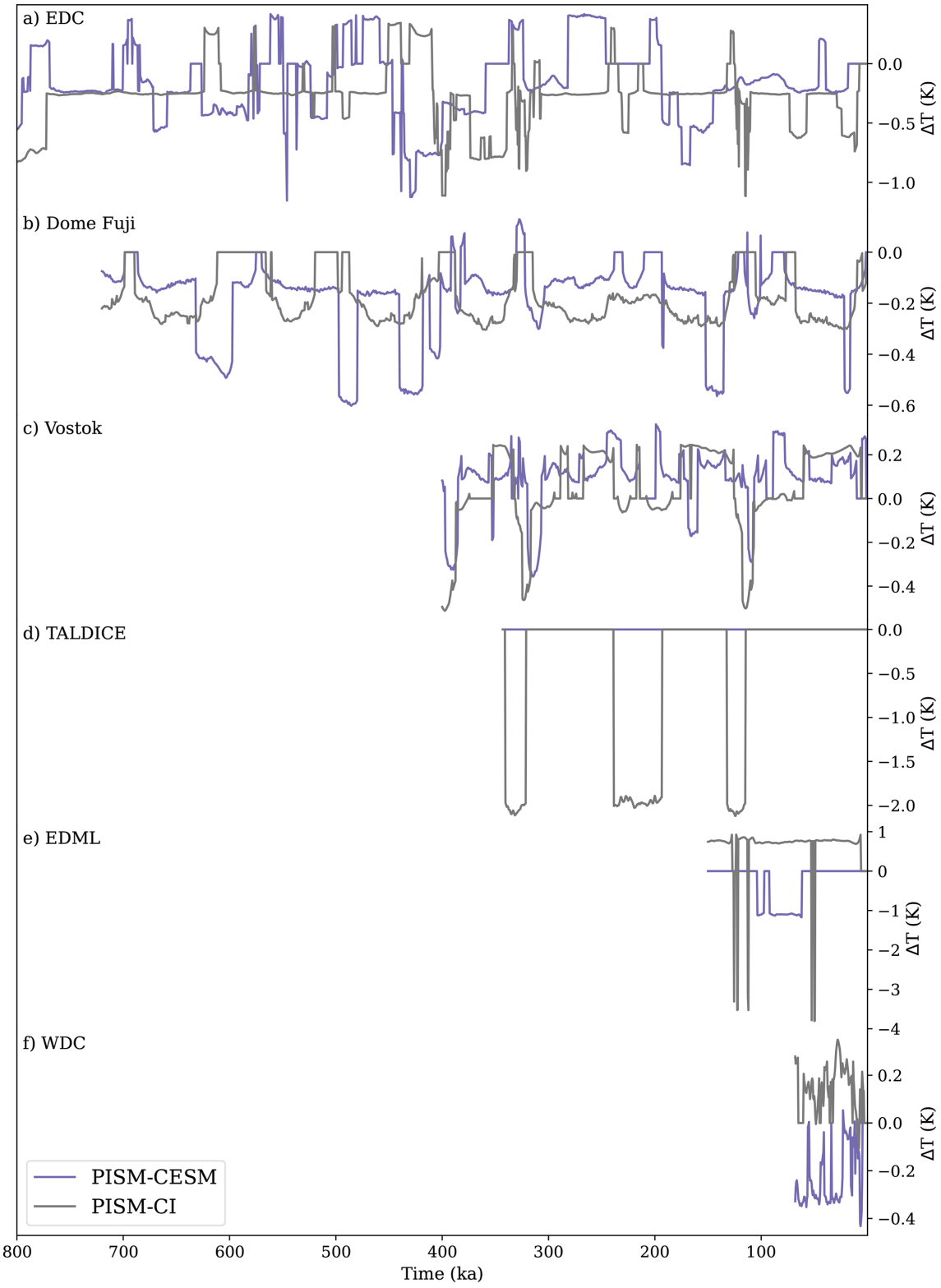


Figure A7. Difference in surface air temperature between the simulated ice-dome position through time and the simulated present-day (fixed) ice-dome position at major Antarctic ice-core locations for PISM-CESM (purple) and PISM-CI (gray). The temperatures are retrieved from the forcing of the respective ice-sheet model simulations.

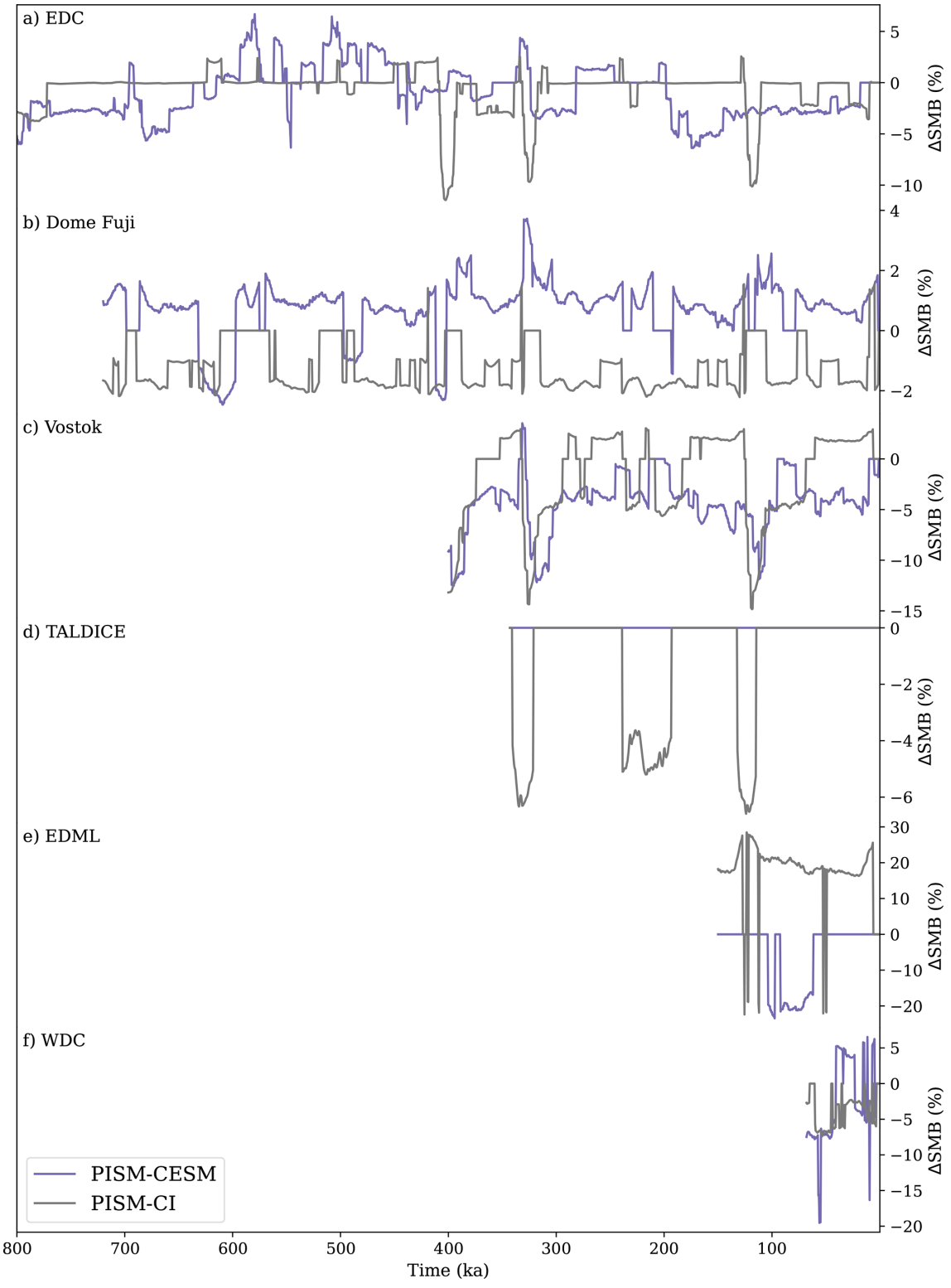


Figure A8. Relative difference in SMB between the simulated ice-dome position through time and the simulated present-day (fixed) ice-dome position at major Antarctic ice-core locations for PISM-CESM (purple) and PISM-CI (gray). The SMB is retrieved from the forcing of the respective ISM simulations.

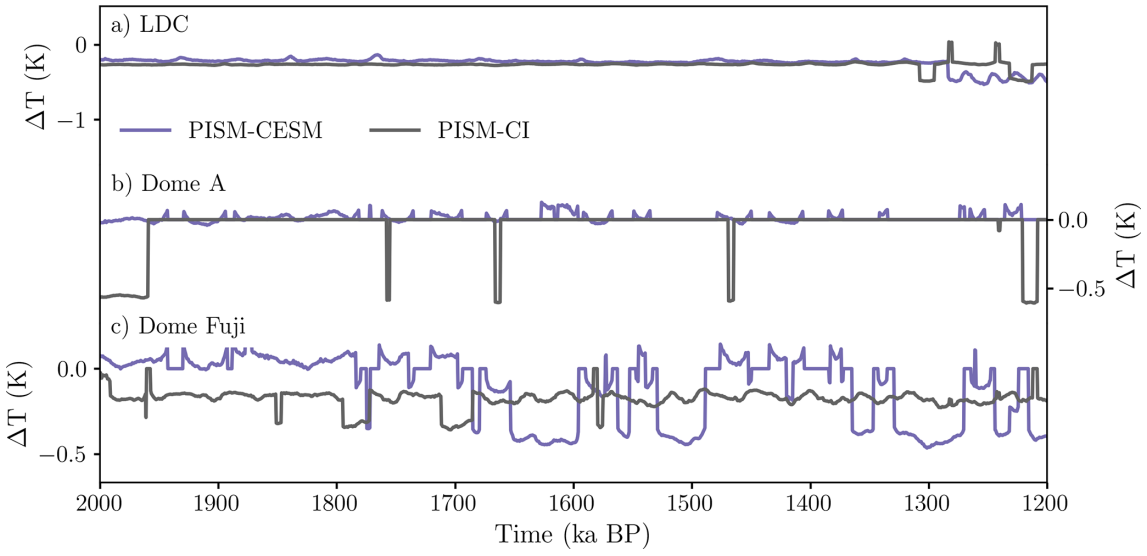


Figure A9. Difference in surface air temperature between the simulated ice-dome position through time and the simulated present-day (fixed) ice-dome position at oldest-ice-core locations for PISM-CESM (purple) and PISM-CI (gray). The temperatures are retrieved from the forcing of the respective ISM simulations.

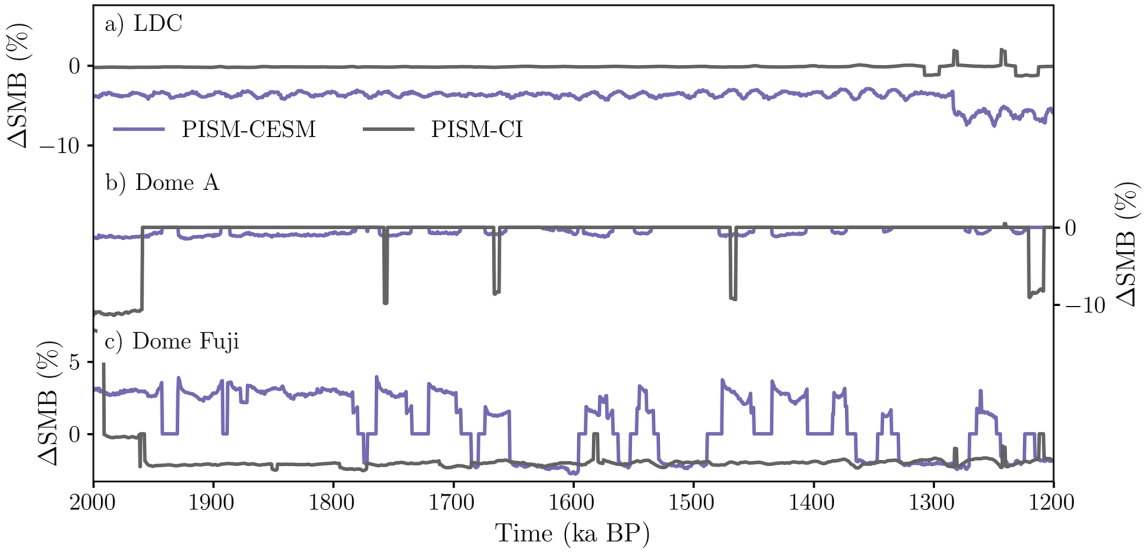


Figure A10. Relative difference in SMB between the simulated ice-dome position through time and the simulated present-day (fixed) ice-dome position at oldest-ice-core locations for PISM-CESM (purple) and PISM-CI (gray). The SMB is retrieved from the forcing of the respective ISM simulations.

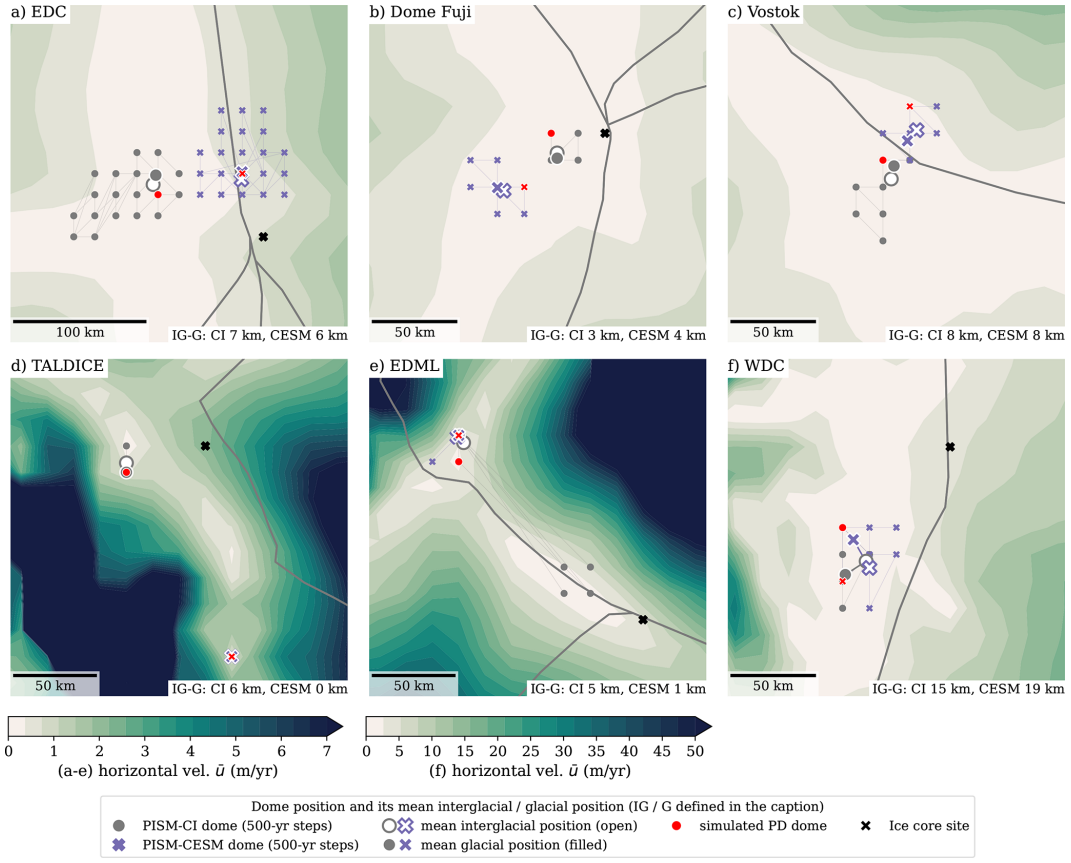


Figure A11. Tracked ice-dome positions at the ice-core sites in 500 year steps for PISM-CI (circles) and PISM-CESM (crosses) over the period covered by the respective ice-core record, as in Fig. 6. Large open and filled markers give the mean dome position of each simulation under interglacial and glacial conditions (δ^{18}O phase angle within ±45° of 0 and 180°, respectively; Sect. 2.2); their separation is annotated in each panel. Red dots mark the simulated present-day dome, black crosses the drill site. Markers overlap where the dome remains within the same grid cell (16 km), so far fewer markers than time steps are visible. Panels are cropped to the area covered by the dome migration; at Vostok the simulated dome lies about 280 km from the drill site, which therefore falls outside the panel.

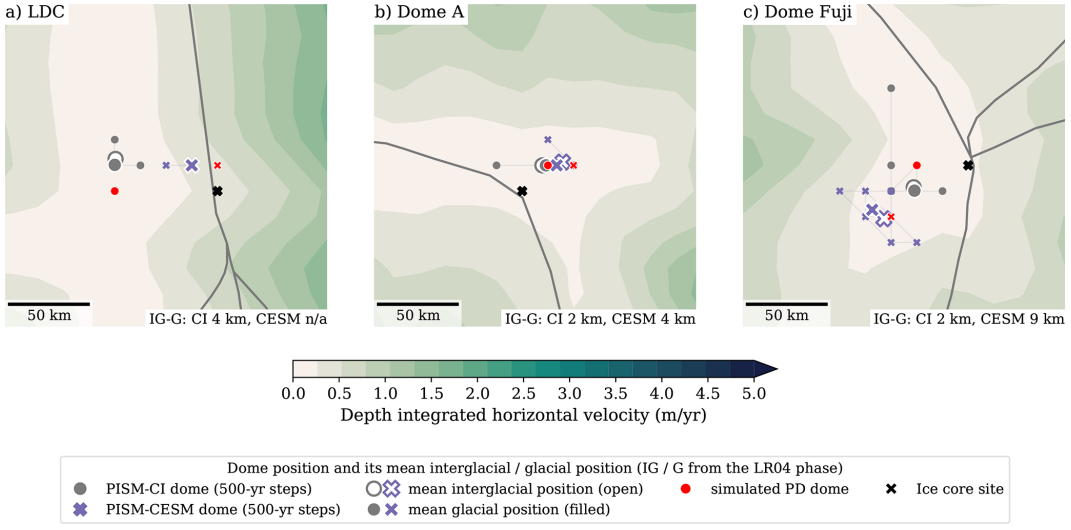


Figure A12. Same as Fig. A11 for the prospective oldest-ice sites between 2.0 and 1.2 Ma BP, as in Fig. 9.

Code and data availability. The PISM model code is publicly available under https://www.pism.io/ (last access: 20 November 2026). The transient Pleistocene 3 Ma model data (10.5194/cp-19-1951-2023, Yun et al., 2023) is available on the OPeNDAP ICCP climate data server https://climatedata.ibs.re.kr (3Ma-Data, 2023; last access: 20 November 2026). The simulated surface elevation anomalies at the ice-core sites, the ice-dome positions and the ice-divide composites presented in this study are available at https://doi.org/10.5281/zenodo.24196550 (Wirths et al., 2026). Codes used in this study are available from the authors upon request.

Author contributions. C.W., A.T., T.F.S., and J.C.R.S. devised the study. K.S.Y. provided the CESM forcing and PSUISM simulation data. C.W. set up the ice-sheet model, preprocessed the forcing, ran the simulations, and performed the analysis. C.W. led the writing of the paper with contributions from all authors.

Competing interests. At least one of the (co-)authors is a member of the editorial board of *The Cryosphere*. The peer-review process was guided by an independent editor, and the authors also have no other competing interests to declare.

Disclaimer. Publisher's note: Copernicus Publications remains neutral with regard to jurisdictional claims made in the text, published maps, institutional affiliations, or any other geographical representation in this paper. The authors bear the ultimate responsibility for providing appropriate place names. Views expressed in the text are those of the authors and do not necessarily reflect the views of the publisher.

Acknowledgements. Calculations were performed on UBELIX, the high-performance computing cluster at the University of Bern. During the preparation of this manuscript, the authors used Claude to assist with language editing, and with reformulating and condensing text passages. All scientific content, analyses, and interpretations originate from the authors, who reviewed and verified all text and take full responsibility for the content of this manuscript.

Financial support. This research has been supported by the Schweizerischer Nationalfonds zur Förderung der Wissenschaftlichen Forschung (grant nos. 200492, 211542, 200020-172506, and 200020B- 200328) and the Institute for Basic Science (grant no. IBS-R028-D1).

Review statement. This paper was edited by Alexander Robinson and reviewed by Fuyuki Saito and one anonymous referee.

References

Ackert, R. P., Barclay, D. J., Borns, H. W., Calkin, P. E., Kurz, M. D., Fastook, J. L., and Steig, E. J.: Measurements of Past Ice Sheet Elevations in Interior West Antarctica, Science, 286, 276–280, https://doi.org/10.1126/science.286.5438.276, 1999.

Anandakrishnan, S., Alley, R. B., and Waddington, E. D.: Sensitivity of the ice-divide position in Greenland to climate change, Geophys. Res. Lett., 21, 441–444, https://doi.org/10.1029/94GL00094, 1994.

Aschwanden, A., Aðalgeirsdóttir, G., and Khroulev, C.: Hindcasting to measure ice sheet model sensitivity to initial states, The Cryosphere, 7, 1083–1093, https://doi.org/10.5194/tc-7-1083-2013, 2013.

Barbante, C. and the Beyond EPICA Team: Beyond EPICA – Oldest Ice Core: Insights from a 1.2-Million-Year-Old Climate Record, EGU General Assembly 2025, Vienna, Austria, 27 Apr–2 May 2025, EGU25-10358, https://doi.org/10.5194/egusphere-egu25-10358, 2025.

Bereiter, B., Eggleston, S., Schmitt, J., Nehrbass-Ahles, C., Stocker, T. F., Fischer, H., Kipfstuhl, S., and Chappellaz, J.: Revision of the EPICA Dome C CO_2 record from 800 to 600 kyr before present, Geophys. Res. Lett., 42, 542–549, https://doi.org/10.1002/2014GL061957, 2015.

Berger, A.: Long-Term Variations of Daily Insolation and Quaternary Climatic Changes, J. Atmos. Sci., 35, 2362–2367, https://doi.org/10.1175/1520-0469(1978)035<2362:LTVODI>2.0.CO;2, 1978.

Bouchet, M., Landais, A., Grisart, A., Parrenin, F., Prié, F., Jacob, R., Fourré, E., Capron, E., Raynaud, D., Lipenkov, V. Y., Loutre, M.-F., Extier, T., Svensson, A., Legrain, E., Martinerie, P., Leuenberger, M., Jiang, W., Ritterbusch, F., Lu, Z.-T., and Yang, G.-M.: The Antarctic Ice Core Chronology 2023 (AICC2023) chronological framework and associated timescale for the European Project for Ice Coring in Antarctica (EPICA) Dome C ice core, Clim. Past, 19, 2257–2286, https://doi.org/10.5194/cp-19-2257-2023, 2023.

Brook, E. J. and Buizert, C.: Antarctic and global climate history viewed from ice cores, Nature, 558, 200–208, https://doi.org/10.1038/s41586-018-0172-5, 2018.

Bueler, E., Lingle, C. S., and Brown, J.: Fast computation of a viscoelastic deformable Earth model for ice-sheet simulations, Ann. Glaciol., 46, 97–105, https://doi.org/10.3189/172756407782871567, 2007.

Buizert, C., Fudge, T. J., Roberts, W. H. G., Steig, E. J., Sherriff-Tadano, S., Ritz, C., Lefebvre, E., Edwards, J., Kawamura, K., Oyabu, I., Motoyama, H., Kahle, E. C., Jones, T. R., Abe-Ouchi, A., Obase, T., Martin, C., Corr, H., Severinghaus, J. P., Beaudette, R., Epifanio, J. A., Brook, E. J., Martin, K., Chappellaz, J., Aoki, S., Nakazawa, T., Sowers, T. A., Alley, R. B., Ahn, J., Sigl, M., Severi, M., Dunbar, N. W., Svensson, A., Fegyveresi, J. M., He, C., Liu, Z., Zhu, J., Otto-Bliesner, B. L., Lipenkov, V. Y., Kageyama, M., and Schwander, J.: Antarctic surface temperature and elevation during the Last Glacial Maximum, Science, 372, 1097–1101, https://doi.org/10.1126/science.abd2897, 2021.

Calov, R. and Greve, R.: A semi-analytical solution for the positive degree-day model with stochastic temperature variations, J. Glaciol., 51, 173–175, https://doi.org/10.3189/172756505781829601, 2005.

Casado, M., Landais, A., Picard, G., Münch, T., Laepple, T., Stenni, B., Dreossi, G., Ekaykin, A., Arnaud, L., Genthon, C., Touzeau, A., Masson-Delmotte, V., and Jouzel, J.: Archival processes of the water stable isotope signal in East Antarctic ice cores, The Cryosphere, 12, 1745–1766, https://doi.org/10.5194/tc-12-1745-2018, 2018.

Cuffey, K. and Paterson, W. S. B.: The physics of glaciers, Butterworth-Heinemann/Elsevier, Burlington, MA, 4th edn., ISBN 978-0-12-369461-4, 2010.

Cuffey, K. M., Clow, G. D., Steig, E. J., Buizert, C., Fudge, T. J., Koutnik, M., Waddington, E. D., Alley, R. B., and Severinghaus, J. P.: Deglacial temperature history of West Antarctica, P. Natl. Acad. Sci. USA, 113, 14249–14254, https://doi.org/10.1073/pnas.1609132113, 2016.

EPICA community members: Eight glacial cycles from an Antarctic ice core, Nature, 429, 623–628, https://doi.org/10.1038/nature02599, 2004.

Fausto, R. S., Ahlstrøm, A. P., As, D. V., Bøggild, C. E., and Johnsen, S. J.: A new present-day temperature parameterization for Greenland, J. Glaciol., 55, 95–105, https://doi.org/10.3189/002214309788608985, 2009.

Fischer, H., Severinghaus, J., Brook, E., Wolff, E., Albert, M., Alemany, O., Arthern, R., Bentley, C., Blankenship, D., Chappellaz, J., Creyts, T., Dahl-Jensen, D., Dinn, M., Frezzotti, M., Fujita, S., Gallee, H., Hindmarsh, R., Hudspeth, D., Jugie, G., Kawamura, K., Lipenkov, V., Miller, H., Mulvaney, R., Parrenin, F., Pattyn, F., Ritz, C., Schwander, J., Steinhage, D., van Ommen, T., and Wilhelms, F.: Where to find 1.5 million yr old ice for the IPICS "Oldest-Ice" ice core, Clim. Past, 9, 2489–2505, https://doi.org/10.5194/cp-9-2489-2013, 2013.

Fudge, T. J., Markle, B. R., Cuffey, K. M., Buizert, C., Taylor, K. C., Steig, E. J., Waddington, E. D., Conway, H., and Koutnik, M.: Variable relationship between accumulation and temperature in West Antarctica for the past 31,000 years, Geophys. Res. Lett., 43, 3795–3803, https://doi.org/10.1002/2016GL068356, 2016.

Gabor, D.: Theory of communication. Part 1: The analysis of information, Journal of the Institution of Electrical Engineers – Part III: Radio and Communication Engineering, 93, 429–441, https://doi.org/10.1049/ji-3-2.1946.0074, 1946.

Golledge, N. R., Fogwill, C. J., Mackintosh, A. N., and Buckley, K. M.: Dynamics of the last glacial maximum Antarctic ice-sheet and its response to ocean forcing, P. Natl. Acad. Sci. USA, 109, 16052–16056, https://doi.org/10.1073/pnas.1205385109, 2012.

Golledge, N. R., Menviel, L., Carter, L., Fogwill, C. J., England, M. H., Cortese, G., and Levy, R. H.: Antarctic contribution to meltwater pulse 1A from reduced Southern Ocean overturning, Nat. Commun., 5, 5107, https://doi.org/10.1038/ncomms6107, 2014.

Goursaud, S., Holloway, M., Sime, L., Wolff, E., Valdes, P., Steig, E. J., and Pauling, A.: Antarctic Ice Sheet Elevation Impacts on Water Isotope Records During the Last Interglacial, Geophys. Res. Lett., 48, e2020GL091412, https://doi.org/10.1029/2020GL091412, 2021.

Hersbach, H., Bell, B., Berrisford, P., Hirahara, S., Horányi, A., Muñoz-Sabater, J., Nicolas, J., Peubey, C., Radu, R., Schepers, D., Simmons, A., Soci, C., Abdalla, S., Abellan, X., Balsamo, G., Bechtold, P., Biavati, G., Bidlot, J., Bonavita, M., De Chiara, G., Dahlgren, P., Dee, D., Diamantakis, M., Dragani, R., Flemming, J., Forbes, R., Fuentes, M., Geer, A., Haimberger, L., Healy, S., Hogan, R. J., Hólm, E., Janisková, M., Keeley, S., Laloyaux, P., Lopez, P., Lupu, C., Radnoti, G., de Rosnay, P., Rozum, I., Vamborg, F., Villaume, S., and Thépaut, J.: The ERA5 global reanalysis, Q. J. Roy. Meteor. Soc., 146, 1999–2049, https://doi.org/10.1002/qj.3803, 2020.

Hindmarsh, R. C. A.: Stochastic perturbation of divide position, Ann. Glaciol., 23, 94–104, https://doi.org/10.3189/S0260305500013306, 1996.

Honari, H., Choe, A. S., and Lindquist, M. A.: Evaluating phase synchronization methods in fMRI: A comparison study and new approaches, NeuroImage, 228, 117704, https://doi.org/10.1016/j.neuroimage.2020.117704, 2021.

Huybrechts, P., Rybak, O., Pattyn, F., Ruth, U., and Steinhage, D.: Ice thinning, upstream advection, and non-climatic biases for the upper 89 % of the EDML ice core from a nested model of the Antarctic ice sheet, Clim. Past, 3, 577–589, https://doi.org/10.5194/cp-3-577-2007, 2007.

Jouzel, J., Masson-Delmotte, V., Cattani, O., Dreyfus, G., Falourd, S., Hoffmann, G., Minster, B., Nouet, J., Barnola, J. M., Chappellaz, J., Fischer, H., Gallet, J. C., Johnsen, S., Leuenberger, M., Loulergue, L., Luethi, D., Oerter, H., Parrenin, F., Raisbeck, G., Raynaud, D., Schilt, A., Schwander, J., Selmo, E., Souchez, R., Spahni, R., Stauffer, B., Steffensen, J. P., Stenni, B., Stocker, T. F., Tison, J. L., Werner, M., and Wolff, E. W.: Orbital and Millennial Antarctic Climate Variability over the Past 800,000 Years, Science, 317, 793–796, https://doi.org/10.1126/science.1141038, 2007.

Kindler, P., Guillevic, M., Baumgartner, M., Schwander, J., Landais, A., and Leuenberger, M.: Temperature reconstruction from 10 to 120 kyr b2k from the NGRIP ice core, Clim. Past, 10, 887–902, https://doi.org/10.5194/cp-10-887-2014, 2014.

Kohfeld, K. E., Graham, R. M., de Boer, A. M., Sime, L. C., Wolff, E. W., Le Quéré, C., and Bopp, L.: Southern Hemisphere westerly wind changes during the Last Glacial Maximum: paleo-data synthesis, Quaternary Sci. Rev., 68, 76–95, https://doi.org/10.1016/j.quascirev.2013.01.017, 2013.

Landais, A., Stenni, B., Masson-Delmotte, V., Jouzel, J., Cauquoin, A., Fourré, E., Minster, B., Selmo, E., Extier, T., Werner, M., Vimeux, F., Uemura, R., Crotti, I., and Grisart, A.: Interglacial Antarctic–Southern Ocean climate decoupling due to moisture source area shifts, Nat. Geosci., 14, 918–923, https://doi.org/10.1038/s41561-021-00856-4, 2021.

Levermann, A., Albrecht, T., Winkelmann, R., Martin, M. A., Haseloff, M., and Joughin, I.: Kinematic first-order calving law implies potential for abrupt ice-shelf retreat, The Cryosphere, 6, 273–286, https://doi.org/10.5194/tc-6-273-2012, 2012.

Li, D., DeConto, R. M., and Pollard, D.: Climate model differences contribute deep uncertainty in future Antarctic ice loss, Science Advances, 9, eadd7082, https://doi.org/10.1126/sciadv.add7082, 2023.

Lisiecki, L. E. and Raymo, M. E.: A Pliocene-Pleistocene stack of 57 globally distributed benthic δ^{18}O records, Paleoceanography, 20, https://doi.org/10.1029/2004PA001071, 2005.

Lüthi, D., Le Floch, M., Bereiter, B., Blunier, T., Barnola, J.-M., Siegenthaler, U., Raynaud, D., Jouzel, J., Fischer, H., Kawamura, K., and Stocker, T. F.: High-resolution carbon dioxide concentration record 650,000–800,000 years before present, Nature, 453, 379–382, https://doi.org/10.1038/nature06949, 2008.

Markle, B. R. and Steig, E. J.: Improving temperature reconstructions from ice-core water-isotope records, Clim. Past, 18, 1321–1368, https://doi.org/10.5194/cp-18-1321-2022, 2022.

Martín, C., Hindmarsh, R. C. A., and Navarro, F. J.: On the effects of divide migration, along-ridge flow, and basal sliding on isochrones near an ice divide, J. Geophys. Res., 114, F02006, https://doi.org/10.1029/2008JF001025, 2009.

Martin, M. A., Winkelmann, R., Haseloff, M., Albrecht, T., Bueler, E., Khroulev, C., and Levermann, A.: The Potsdam Parallel Ice Sheet Model (PISM-PIK) – Part 2: Dynamic equilibrium simulation of the Antarctic ice sheet, The Cryosphere, 5, 727–740, https://doi.org/10.5194/tc-5-727-2011, 2011.

Mengel, M. and Levermann, A.: Ice plug prevents irreversible discharge from East Antarctica, Nat. Clim. Change, 4, 451–455, https://doi.org/10.1038/nclimate2226, 2014.

Morlighem, M., Rignot, E., Binder, T., Blankenship, D., Drews, R., Eagles, G., Eisen, O., Ferraccioli, F., Forsberg, R., Fretwell, P., Goel, V., Greenbaum, J. S., Gudmundsson, H., Guo, J., Helm, V., Hofstede, C., Howat, I., Humbert, A., Jokat, W., Karlsson, N. B., Lee, W. S., Matsuoka, K., Millan, R., Mouginot, J., Paden, J., Pattyn, F., Roberts, J., Rosier, S., Ruppel, A., Seroussi, H., Smith, E. C., Steinhage, D., Sun, B., Broeke, M. R. v. d., Ommen, T. D. v., Wessem, M. v., and Young, D. A.: Deep glacial troughs and stabilizing ridges unveiled beneath the margins of the Antarctic ice sheet, Nat. Geosci., 13, 132–137, https://doi.org/10.1038/s41561-019-0510-8, 2020.

Nereson, N. A., Raymond, C. F., Waddington, E. D., and Jacobel, R. W.: Migration of the Siple Dome ice divide, West Antarctica, J. Glaciol., 44, 643–652, https://doi.org/10.3189/S0022143000002148, 1998.

Noone, D. and Simmonds, I.: Sea ice control of water isotope transport to Antarctica and implications for ice core interpretation, J. Geophys. Res.-Atmos., 109, https://doi.org/10.1029/2003JD004228, 2004.

Nowicki, S., Goelzer, H., Seroussi, H., Payne, A. J., Lipscomb, W. H., Abe-Ouchi, A., Agosta, C., Alexander, P., Asay-Davis, X. S., Barthel, A., Bracegirdle, T. J., Cullather, R., Felikson, D., Fettweis, X., Gregory, J. M., Hattermann, T., Jourdain, N. C., Kuipers Munneke, P., Larour, E., Little, C. M., Morlighem, M., Nias, I., Shepherd, A., Simon, E., Slater, D., Smith, R. S., Straneo, F., Trusel, L. D., van den Broeke, M. R., and van de Wal, R.: Experimental protocol for sea level projections from ISMIP6 stand-alone ice sheet models, The Cryosphere, 14, 2331–2368, https://doi.org/10.5194/tc-14-2331-2020, 2020.

Parrenin, F., Barnola, J.-M., Beer, J., Blunier, T., Castellano, E., Chappellaz, J., Dreyfus, G., Fischer, H., Fujita, S., Jouzel, J., Kawamura, K., Lemieux-Dudon, B., Loulergue, L., Masson-Delmotte, V., Narcisi, B., Petit, J.-R., Raisbeck, G., Raynaud, D., Ruth, U., Schwander, J., Severi, M., Spahni, R., Steffensen, J. P., Svensson, A., Udisti, R., Waelbroeck, C., and Wolff, E.: The EDC3 chronology for the EPICA Dome C ice core, Clim. Past, 3, 485–497, https://doi.org/10.5194/cp-3-485-2007, 2007a.

Parrenin, F., Dreyfus, G., Durand, G., Fujita, S., Gagliardini, O., Gillet, F., Jouzel, J., Kawamura, K., Lhomme, N., Masson-Delmotte, V., Ritz, C., Schwander, J., Shoji, H., Uemura, R., Watanabe, O., and Yoshida, N.: 1-D-ice flow modelling at EPICA Dome C and Dome Fuji, East Antarctica, Clim. Past, 3, 243–259, https://doi.org/10.5194/cp-3-243-2007, 2007b.

Parrenin, F., Fujita, S., Abe-Ouchi, A., Kawamura, K., Masson-Delmotte, V., Motoyama, H., Saito, F., Severi, M., Stenni, B., Uemura, R., and Wolff, E. W.: Climate dependent contrast in surface mass balance in East Antarctica over the past 216 ka, J. Glaciol., 62, 1037–1048, https://doi.org/10.1017/jog.2016.85, 2016.

Pfeiffer, M. and Lohmann, G.: Greenland Ice Sheet influence on Last Interglacial climate: global sensitivity studies performed with an atmosphere–ocean general circulation model, Clim. Past, 12, 1313–1338, https://doi.org/10.5194/cp-12-1313-2016, 2016.

Pollard, D. and DeConto, R. M.: Modelling West Antarctic ice sheet growth and collapse through the past five million years, Nature, 458, 329–332, https://doi.org/10.1038/nature07809, 2009.

Pollard, D. and DeConto, R. M.: Description of a hybrid ice sheet-shelf model, and application to Antarctica, Geosci. Model Dev., 5, 1273–1295, https://doi.org/10.5194/gmd-5-1273-2012, 2012a.

Pollard, D. and DeConto, R. M.: A simple inverse method for the distribution of basal sliding coefficients under ice sheets, applied to Antarctica, The Cryosphere, 6, 953–971, https://doi.org/10.5194/tc-6-953-2012, 2012b.

Pollard, D., DeConto, R. M., and Alley, R. B.: Potential Antarctic Ice Sheet retreat driven by hydrofracturing and ice cliff failure, Earth Planet. Sc. Lett., 412, 112–121, https://doi.org/10.1016/j.epsl.2014.12.035, 2015.

Reese, R., Albrecht, T., Mengel, M., Asay-Davis, X., and Winkelmann, R.: Antarctic sub-shelf melt rates via PICO, The Cryosphere, 12, 1969–1985, https://doi.org/10.5194/tc-12-1969-2018, 2018.

Rieckh, T., Born, A., Robinson, A., Law, R., and Gülle, G.: Design and performance of ELSA v2.0: an isochronal model for ice-sheet layer tracing, Geosci. Model Dev., 17, 6987–7000, https://doi.org/10.5194/gmd-17-6987-2024, 2024.

Rignot, E., Mouginot, J., and Scheuchl, B.: Ice Flow of the Antarctic Ice Sheet, Science, 333, 1427–1430, https://doi.org/10.1126/science.1208336, 2011.

Risi, C., Bony, S., Vimeux, F., and Jouzel, J.: Water-stable isotopes in the LMDZ4 general circulation model: Model evaluation for present-day and past climates and applications to climatic interpretations of tropical isotopic records, J. Geophys. Res.-Atmos., 115, https://doi.org/10.1029/2009JD013255, 2010.

Ritz, C., Rommelaere, V., and Dumas, C.: Modeling the evolution of Antarctic ice sheet over the last 420,000 years: Implications for altitude changes in the Vostok region, J. Geophys. Res.-Atmos., 106, 31943–31964, https://doi.org/10.1029/2001JD900232, 2001.

Robinson, A., Calov, R., and Ganopolski, A.: An efficient regional energy-moisture balance model for simulation of the Greenland Ice Sheet response to climate change, The Cryosphere, 4, 129–144, https://doi.org/10.5194/tc-4-129-2010, 2010.

Schoof, C.: Ice sheet grounding line dynamics: Steady states, stability, and hysteresis, J. Geophys. Res.-Earth, 112, https://doi.org/10.1029/2006JF000664, 2007.

Schwander, J. and Stauffer, B.: Age difference between polar ice and the air trapped in its bubbles, Nature, 311, 45–47, https://doi.org/10.1038/311045a0, 1984.

Severinghaus, J. P., Sowers, T., Brook, E. J., Alley, R. B., and Bender, M. L.: Timing of abrupt climate change at the end of the Younger Dryas interval from thermally fractionated gases in polar ice, Nature, 391, 141–146, 1998.

Shapiro, N. M. and Ritzwoller, M. H.: Inferring surface heat flux distributions guided by a global seismic model: particular application to Antarctica, Earth Planet. Sc. Lett., 223, 213–224, https://doi.org/10.1016/j.epsl.2004.04.011, 2004.

Steig, E. J., Fastook, J. L., Zweck, C., Goodwin, I. D., Licht, K. J., White, J. W. C., and Ackert, R. P.: West Antarctic Ice Sheet Elevation Changes, in: Antarctic Research Series, American Geophysical Union, Washington, D. C., 75–90, ISBN 978-1-118-66832-0 978-0-87590-957-8, https://doi.org/10.1029/AR077p0075, 2001.

Stenni, B., Masson-Delmotte, V., Selmo, E., Oerter, H., Meyer, H., Röthlisberger, R., Jouzel, J., Cattani, O., Falourd, S., Fischer, H., Hoffmann, G., Iacumin, P., Johnsen, S. J., Minster, B., and Udisti, R.: The deuterium excess records of EPICA Dome C and Dronning Maud Land ice cores (East Antarctica), Quaternary Sci. Rev., 29, 146–159, https://doi.org/10.1016/j.quascirev.2009.10.009, 2010.

Stepanek, C. and Lohmann, G.: Modelling mid-Pliocene climate with COSMOS, Geosci. Model Dev., 5, 1221–1243, https://doi.org/10.5194/gmd-5-1221-2012, 2012.

Stepanek, C., Samakinwa, E., Knorr, G., and Lohmann, G.: Contribution of the coupled atmosphere–ocean–sea ice–vegetation model COSMOS to the PlioMIP2, Clim. Past, 16, 2275–2323, https://doi.org/10.5194/cp-16-2275-2020, 2020.

Sutter, J., Fischer, H., Grosfeld, K., Karlsson, N. B., Kleiner, T., Van Liefferinge, B., and Eisen, O.: Modelling the Antarctic Ice Sheet across the mid-Pleistocene transition – implications for Oldest Ice, The Cryosphere, 13, 2023–2041, https://doi.org/10.5194/tc-13-2023-2019, 2019.

Tigchelaar, M., Timmermann, A., Pollard, D., Friedrich, T., and Heinemann, M.: Local insolation changes enhance Antarctic interglacials: Insights from an 800,000-year ice sheet simulation with transient climate forcing, Earth Planet. Sc. Lett., 495, 69–78, https://doi.org/10.1016/j.epsl.2018.05.004, 2018.

van Dalum, C. T., van de Berg, W. J., and van den Broeke, M. R.: Sensitivity of Antarctic surface climate to a new spectral snow albedo and radiative transfer scheme in RACMO2.3p3, The Cryosphere, 16, 1071–1089, https://doi.org/10.5194/tc-16-1071-2022, 2022.

Wang, Q.-X., Li, T., Cheng, X., Zhao, C., Zheng, L., and Liang, Q.: Exploring grid sensitivity in an ice sheet model: A case study of the Amery Ice Shelf, Advances in Climate Change Research, 15, 1013–1026, https://doi.org/10.1016/j.accre.2024.12.001, 2024.

Weertman, J.: Position of ice divides and ice centers on ice sheets, J. Glaciol., 12, 353–360, https://doi.org/10.3189/S0022143000031774, 1973.

Werner, M., Jouzel, J., Masson-Delmotte, V., and Lohmann, G.: Reconciling glacial Antarctic water stable isotopes with ice sheet topography and the isotopic paleothermometer, Nat. Commun., 9, 3537, https://doi.org/10.1038/s41467-018-05430-y, 2018.

Willeit, M., Ganopolski, A., Calov, R., and Brovkin, V.: Mid-Pleistocene transition in glacial cycles explained by declining CO2 and regolith removal, Science Advances, 5, eaav7337, https://doi.org/10.1126/sciadv.aav7337, 2019.

Winkelmann, R., Martin, M. A., Haseloff, M., Albrecht, T., Bueler, E., Khroulev, C., and Levermann, A.: The Potsdam Parallel Ice Sheet Model (PISM-PIK) – Part 1: Model description, The Cryosphere, 5, 715–726, https://doi.org/10.5194/tc-5-715-2011, 2011.

Wirths, C., Stocker, T. F., and Sutter, J. C. R.: The influence of present-day regional surface mass balance uncertainties on the future evolution of the Antarctic Ice Sheet, The Cryosphere, 18, 4435–4462, https://doi.org/10.5194/tc-18-4435-2024, 2024.

Wirths, C., Hermant, A., Stepanek, C., Stocker, T. F., and Sutter, J. C. R.: Sequence of abrupt transitions in Antarctic drainage basins before and during the Mid-Pleistocene Transition, Nat. Commun., 16, https://doi.org/10.1038/s41467-025-65375-x, 2025.

Wirths, C., Yun, K.-S., Timmermann, A., Fischer, H., Stocker, T. F., and Sutter, J. C. R.: Data for "Estimating the impact of ice-sheet surface height and ice-divide variability on ice-core based climate reconstructions", Zenodo [data set], https://doi.org/10.5281/zenodo.24196550, 2026.

Yun, K.-S. and Timmermann, A.: Increased sensitivity of the Antarctic Ice Sheet to decreasing CO2 across the Mid-Pleistocene Transition, Nat. Geosci., 19, 683–690, https://doi.org/10.1038/s41561-026-01979-2, 2026.

Yun, K.-S., Timmermann, A., Lee, S.-S., Willeit, M., Ganopolski, A., and Jadhav, J.: A transient coupled general circulation model (CGCM) simulation of the past 3 million years, Clim. Past, 19, 1951–1974, https://doi.org/10.5194/cp-19-1951-2023, 2023.

Zhang, X., Lohmann, G., Knorr, G., and Xu, X.: Different ocean states and transient characteristics in Last Glacial Maximum simulations and implications for deglaciation, Clim. Past, 9, 2319–2333, https://doi.org/10.5194/cp-9-2319-2013, 2013.